Dysregulated *H19/Igf2* expression disrupts cardiac-placental axis during development of Silver Russell Syndrome-like mouse models

Suhee Chang[1], Diana Fulmer[1,2], Stella K. Hur[1], Joanne L. Thorvaldsen[1], Li Li[1,2], Yemin Lan[1], Eric A. Rhon-Calderon[1], N Adrian Leu[3], Xiaowen Chen[2], Jonathan A. Epstein[1,2], Marisa S. Bartolomei[1]

[1]Department of Cell and Developmental Biology, Epigenetics Institute, Perelman School of Medicine, University of Pennsylvania, Philadelphia, PA, United States

[2]Penn Cardiovascular Institute, Perelman School of Medicine, University of Pennsylvania, Philadelphia, PA, United States

[3]Department of Biomedical Sciences, School of Veterinary Medicine, Institute for Regenerative Medicine, University of Pennsylvania, Philadelphia, PA, United States

[*Keywords*: *H19*; *Igf2*; SRS; cardiac development; cardiac-placental axis; VSD; ECM; endothelial cells]

Corresponding author: bartolom@pennmedicine.upenn.edu

Abstract

Dysregulation of the imprinted *H19/IGF2* locus can lead to Silver-Russell Syndrome (SRS) in humans. However, the mechanism of how abnormal *H19/IGF2* expression contributes to various SRS phenotypes remains unclear, largely due to incomplete understanding of the developmental functions of these two genes. We previously generated a mouse model with humanized *H19/IGF2* ICR (*hIC1*) on the paternal allele that exhibited *H19/Igf2* dysregulation together with SRS-like growth restriction and perinatal lethality. Here we dissect the role of *H19* and *Igf2* in cardiac and placental development utilizing multiple mouse models with varying levels of *H19* and *Igf2*. We report severe cardiac defects such as ventricular septal defects (VSDs) and thinned myocardium, placental anomalies including thrombosis and vascular malformations, together with growth restriction in mouse embryos that correlated with the extent of *H19/Igf2* dysregulation. Transcriptomic analysis using cardiac endothelial cells of these mouse models shows that *H19/Igf2* dysregulation disrupts pathways related to extracellular matrix (ECM) and proliferation of endothelial cells. Our work links the heart and placenta through regulation by *H19* and *Igf2*, demonstrating that accurate dosage of both *H19* and *Igf2* is critical for normal embryonic development, especially related to the cardiac-placental axis.

Introduction

Genomic imprinting is a mammalian-specific phenomenon where a small number of genes are expressed in an allele-specific manner. Functionally, imprinted genes have central roles in development and growth in both humans and mice (Barlow & Bartolomei, 2014). Additionally, proper gene dosage of most imprinted genes is essential for normal development. Human chromosome 11 and the orthologous region on mouse chromosome 7 harbor two jointly controlled growth regulators with opposing functions; *H19* long noncoding RNA (lncRNA) and Insulin-like Growth Factor 2 (*IGF2/Igf2)*. These two imprinted genes share an imprinting control region (ICR), a *cis*-regulatory element located between two genes, which is essential for their allele-specific expression, as well as tissue-specific enhancers located

downstream of *H19* (Chang & Bartolomei, 2020). The *H19/IGF2* ICR, which is designated as IC1 in humans, binds CTCF on the maternal allele, forming an insulator and enabling *H19* exclusive access to the shared enhancers (Figure 1A). On the paternal allele, the *H19/IGF2* ICR is methylated, which prevents CTCF from binding and an insulator from forming. Consequently, *IGF2* usurps the shared enhancers and *H19* is repressed on the paternal allele. Ultimately, allele-specific ICR methylation facilitates monoallelic expression of *H19* and *IGF2* with *H19* expressed from the maternal allele and *IGF2* expressed from the paternal allele.

Dysregulation of the *H19/IGF2* cluster is associated with two growth disorders, Beckwith-Wiedemann Syndrome (BWS) and Silver-Russell Syndrome (SRS). In contrast to overgrowth observed for BWS, SRS is characterized by intrauterine growth restriction resulting in small for gestational age (SGA) births. Other symptoms of SRS vary widely among patients and include hemihypotrophy, cognitive impairment, relative macrocephaly, and fifth-finger clinodactyly (Wakeling et al., 2017). Approximately 50% of patients with SRS exhibit IC1 hypomethylation (Eggermann et al., 2011). Lack of methylation may allow the formation of an ectopic insulator on paternal IC1, which likely explains why this class of SRS individuals has biallelic *H19* expression and greatly diminished *IGF2* expression (Abi Habib et al., 2017; Gicquel et al., 2005). Importantly, ICR mutations in the mouse that were generated to study imprinted gene regulation provided critical information suggesting a role for *H19* and *IGF2* in SRS. For example, mutating CpGs at CTCF sites on the paternal *H19/Igf2* ICR resulted in the loss of ICR methylation, activation of paternal *H19* and reduced *Igf2* expression (Engel et al., 2004). This mutation led to restricted embryonic growth, which phenocopies SRS. Nevertheless, although we and others successfully modeled a subset of SRS mutations in the mouse, not all mutations were translatable because the mouse *H19*/*Igf2* ICR lacks extensive sequence conservation with human IC1. Thus, a mouse model with human IC1 sequence substituted for the endogenous mouse *H19*/*Igf2* ICR was generated ($H19^{hIC1}$, shortened as *hIC1*; Hur et al., 2016) to model human mutations more precisely (Freschi et al., 2018, 2021). Consistent with expectations, maternally transmitted *hIC1* successfully maintained insulator function, suggesting the possibility to model human IC1 mutations endogenously in mice upon maternal

transmission. In contrast, paternally transmitted *hIC1* showed loss of methylation and formation of an ectopic insulator. Consequently, paternal *hIC1* transmission caused elevated *H19* expression and *Igf2* depletion together with growth restriction and embryonic lethality (Hur et al., 2016). Although the epigenetic defects and growth restriction of these mice nicely model SRS symptoms, many SRS individuals are viable. A potential explanation for such discrepancy between human and mouse could reflect the mosaic nature of epigenetic defects in human (Soellner et al., 2019), with a subset of cells showing normal methylation patterns.

The mechanism by which *H19/IGF2* expression dysregulation causes SRS phenotypes is unknown, largely because the function of these two genes during development is incompletely understood. *IGF2* is a well-described growth factor promoting fetoplacental growth, which functions in an endocrine/paracrine manner through binding to IGF/Insulin receptors (Harris & Westwood, 2012). Decreased *IGF2* levels in patients with SRS suggests that IGF2 contributes to restricted growth in these patients (Abi Habib et al., 2017; Begemann et al., 2015; Gicquel et al., 2005). Consistently, in mice, paternal-specific deletion of *Igf2* resulted in loss of *Igf2* expression and pre- and postnatal growth restriction (DeChiara et al., 1991; Haley et al., 2012). In contrast, the exact role of *H19* remains unclear. Previous studies in mouse suggested that *H19* lncRNA is a precursor for microRNA (miR)-675, which regulates *Igf1r* expression (Keniry et al., 2012), and that *H19* represses *Igf2* expression *in trans* (Gabory et al., 2009). As a result, *H19* has been largely overlooked and suggested to be an occasional regulator of *Igf2* expression. Nevertheless, a previously described mouse model with *H19* overexpression without changes in *Igf2* expression showed embryonic growth restriction (Drewell et al., 2000), suggesting that *H19* mediates growth suppression independently from *Igf2*. Here, we report severe developmental defects of the heart and placenta in mouse models with dysregulated *H19/Igf2* expression. Embryos with the paternal *hIC1* showed atrioventricular (AV) cushion defects in the heart coupled with ventricular septal defects (VSDs), and extremely thinned myocardial walls. Combined with placental anomalies, the cardiac defects most likely contribute to the lethality of these mice (Kochilas et al., 1999; Snider & Conway, 2011). Deletion of *H19* from the maternal allele, thereby reducing *H19* levels, failed to rescue completely

the lethality and growth restriction associated with the paternal inheritance of *hIC1*. A minimal rescue of the earlier growth and resorption frequency was, however, observed with normalized *H19* expression. Ultimately, modifying both *H19* and *Igf2* expression was necessary to rescue most phenotypes. Transcriptomic analysis of embryonic cardiac endothelial cells identified several key signaling pathways that are affected by the dysregulated *H19* and *Igf2*, and are potentially responsible for the paternal *hIC1*-related cardiac defects. This work emphasizes the importance of accurate dosage of *H19* and *Igf2* expression in normal cardiac and placental development, disruption of which can lead to SRS-like pathologies.

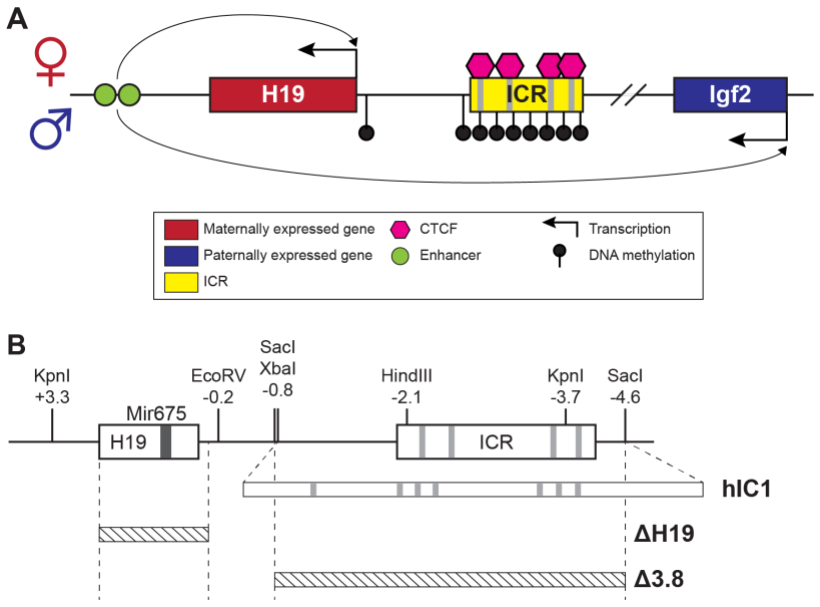

Figure 1. *H19/Igf2* cluster and mouse models utilized in this study.
(A) A schematic representation of the wild-type *H19/Igf2* cluster in mouse. The maternally-expressed *H19* and the paternally-expressed *Igf2* genes are shown in red and blue, respectively. Black lollipops on the paternal allele represent DNA methylation. The maternal ICR is bound to CTCF proteins (pink hexagons) at CTCF binding sites, forming an insulator that blocks the maternal *Igf2* promoter from the shared enhancers (green circles). These enhancers interact with the *H19* promoter on the maternal allele and *Igf2* promoter on the paternal allele. (B) Schematic of the mouse endogenous *H19/Igf2* ICR, $H19^{hIC1}$ (shortened as *hIC1*; Hur et al. 2016), $H19^{\triangle 2.8kb\text{-}H19}$ (shortened as *△H19*), and $H19^{\triangle 3.8kb\text{-}5'H19}$ (shortened as *△3.8*; Thorvaldsen et al. 2002, 2006) alleles. Restriction site locations (kb) are relative to the *H19* transcription start site. Gray lines on the ICR represent conserved CTCF binding sequences.

Results

Mouse models with genetic modifications that perturb *H19* and *Igf2* to different extents were used to address the phenotypic consequences of abnormal *H19* and *Igf2* levels (Figure 1B). *hIC1* refers to the humanized $H19^{hIC1}$ allele that substitutes the endogenous mouse *H19/Igf2* ICR with the corresponding human IC1 sequence, which was initially generated to study human BWS and SRS mutations in the mouse (Freschi et al., 2018; Hur et al., 2016). Paternal transmission of *hIC1* [*+/hIC1*] was previously reported to increase *H19* and greatly diminish *Igf2* expression and resulted in embryonic lethality.

Cardiac and placental defects in *+/hIC1* embryos

Our initial experiments examined the developmental phenotype of *+/hIC1* embryos to determine how abnormal *H19/Igf2* expression resulted in dramatic growth defects and lethality. As previously reported (Hur et al., 2016), *+/hIC1* embryos showed severe growth restriction (note that for heterozygous embryos, maternal allele is written first, Figure 2A). The growth restriction appeared as early as E11.5 and was greatly exaggerated by the end of gestation. Although E18.5 *+/hIC1* embryos were observed alive and weighed approximately 40% of their wild-type littermates, *+/hIC1* neonates were perinatally lethal, with no live pups found on the day of birth. To ascertain the source of lethality, we first examined lungs from dead *+/hIC1* neonates. The lungs floated in water, demonstrating that *+/hIC1* pups respired after birth (Borensztein et al., 2012). Additionally, *+/hIC1* neonates did not have a cleft palate, but no milk spots were found in their abdomen, indicating a lack of feeding.

Histological analyses were performed throughout development on major organs where *H19* and *Igf2* are highly expressed. Severe developmental defects were found in the *+/hIC1* heart and placenta. Cardiac defects in *+/hIC1* embryos were observed as early as E12.5, where the superior and inferior endocardial cushions failed to fuse into a common AV cushion (Figure 2C). The cushion defect preceded incomplete interventricular septum (IVS) formation. At E15.5, a severe perimembranous ventricular septal defect (VSD) was observed in all 5 *+/hIC1* hearts that were evaluated (Figure 2C). Importantly, this congenital heart defect resembles malformations reported in several SRS patients with IC1

hypomethylation (Ghanim et al., 2013), although the prevalence is unclear and may reflect the degree of mosaicism in SRS. Additionally, E15.5 hearts showed an extremely thin myocardium (Figure 2C and Supplemental Figure 1A). Both VSD and thinned ventricular walls persisted in E17.5 *+/hIC1* hearts (Figure 2B and C). Additionally, 6 out of 16 *+/hIC1* hearts in the late gestation group (E15.5 to P0) had bicuspid pulmonary valve (BPV), a rare cardiac defect in which the pulmonary valve only develops two cusps as opposed to the normal tricuspid structure (Figure 2D and Supplemental Figure 2). These results demonstrate that paternal *hIC1* transmission results in variably penetrant cardiac phenotypes. Notably, atrioventricular valvuloseptal morphogenesis, the fusion of the AV cushion and nascent septa during cardiogenesis, is required for proper cardiac septation (Eisenberg & Markwald, 1995). Segmentation of the heart into four separate chambers is required to establish distinct pulmonary and systemic blood flow during heart development and is required to prevent the mixing of oxygenated and deoxygenated blood. We speculate that the failure of *hIC1* mutants to establish complete ventricular septation could have led to a reduced ability to provide oxygen and nutrient rich blood to the rest of the developing body (Savolainen et al., 2009; Spicer et al., 2014).

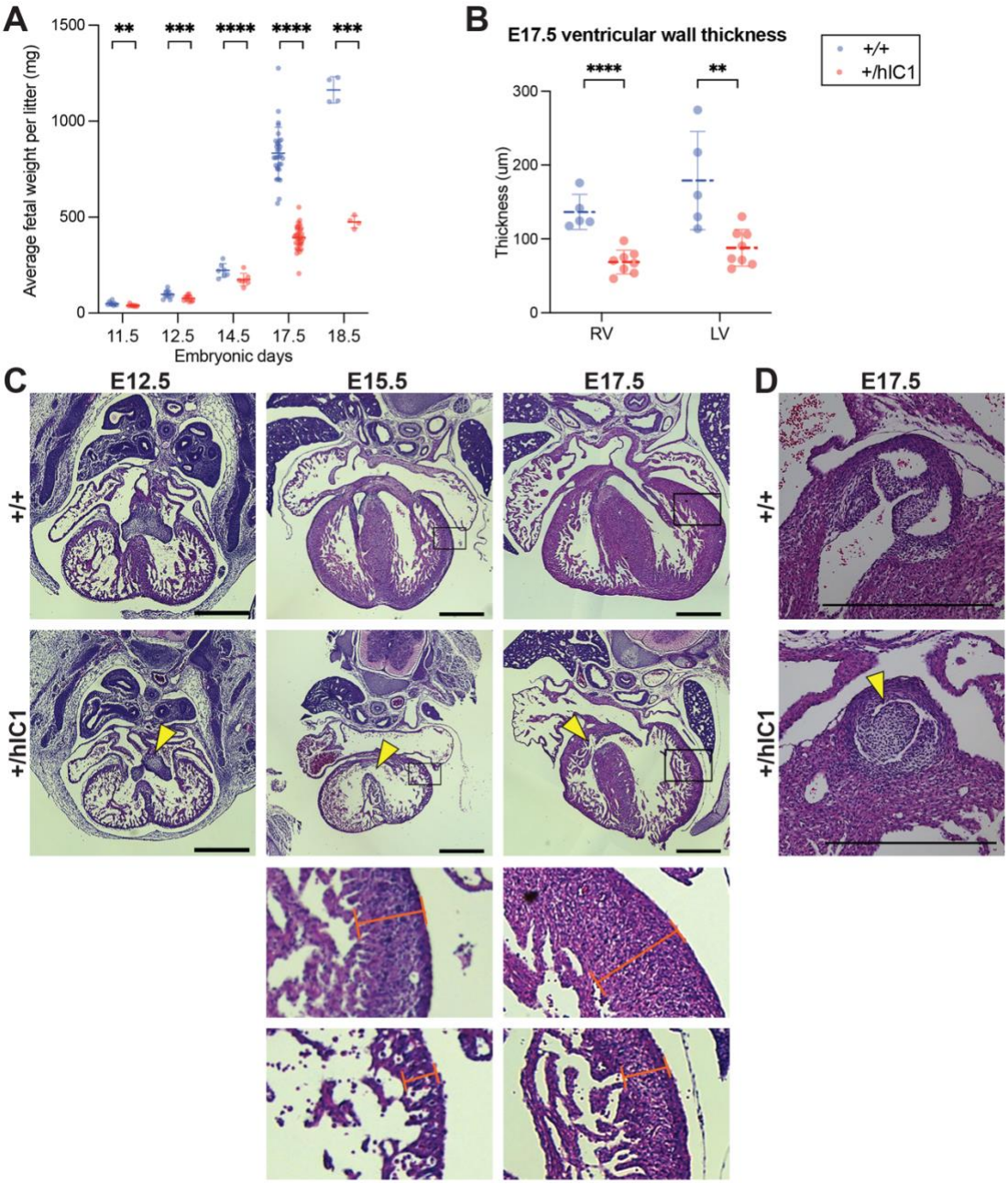

145

Figure 2. Growth anomalies and cardiac defects of *+/hIC1* embryos.

(A) Fetal weight of the wild-type (blue) and *+/hIC1* (red) embryos at E11.5, E12.5, E14.5, E17.5 and E18.5 (mean ± SD). Each data point represents an average weight of each genotype from one litter. 8 litters for E11.5, 10 litters for E12.5, 7 litters for E14.5, 31 litters for E17.5, 4 litters for E18.5 are presented. (B) Quantification of ventricular wall thickness (μm), measured from E17.5 wild-type and *+/hIC1* hearts (mean ± SD). Each data point represents an individual conceptus. 5 wild-type and 8 *+/hIC1* embryos from four different litters were examined. (C) Representative cross-sections of wild-type and *+/hIC1* embryonic hearts at E12.5, E15.5 and E17.5, stained with hematoxylin and eosin. All the hearts represented here are from female fetuses. Note the lack of fusion between AV cushions at

E12.5, the VSD at E15.5 and E17.5 in *+/hIC1* hearts (yellow arrowheads). The boxed regions of E15.5 and E17.5 images are enlarged at the bottom of the figure, to show where the ventricular wall thickness is measured. Scale bars = 500 µm. (D) A representative image of pulmonary valves in E17.5 wild-type and *+/hIC1* hearts. The *+/hIC1* right pulmonary cusp is enlarged (yellow arrowhead) and there is no cusp in the anterior position, in contrast to the tricuspid structure in the wild-type heart. Scale bars = 500 µm. Statistics used are (A) multiple paired t-test and (B) multiple unpaired t-test with $^{**}P < 0.01$, $^{***}P < 0.001$, $^{****}P < 0.0001$ and ns = not significant.

Another major organ with high *H19/Igf2* expression, which forms early in development, is the placenta. Multiple developmental defects were observed in *+/hIC1* placentas. As previously described (Hur et al., 2016), *+/hIC1* placentas were growth restricted throughout development (Figure 3A), although the fetal to placental weight ratio was not affected through E15.5 (Supplemental Figure 1B). However, at E17.5, the fetal to placental weight ratio was lower in *+/hIC1* conceptuses, indicating that the fetal growth restriction was more severe than the placental growth restriction as the concepti neared term (Figure 3B). In addition to placental undergrowth, the junctional to labyrinth zone ratio was increased in *+/hIC1* placentas (Figure 3C and Supplemental Figure 1C), suggesting that the growth of the labyrinth layer, where the maternal-fetal exchange occurs, was more affected. Moreover, *H19* overexpression was exaggerated in the labyrinth in E17.5 *+/hIC1* placentas, while the *Igf2* depletion was consistent throughout the whole placenta (Figure 3D), possibly indicating that *H19* overexpression contributed disproportionately to the phenotype of growth restriction in the labyrinth. Large thrombi were observed in the labyrinth zone of these *+/hIC1* placentas (Figure 3F), in a male-skewed manner (Figure 3E). As the thrombi could be formed due to defective vasculature structures, wild-type and *+/hIC1* placentas were stained for CD34, a marker for the fetoplacental endothelial cells that line the microvessels in the labyrinth layer. Vessels in the *+/hIC1* labyrinth were highly dilated (Figure 3G), and quantification of the stained areas showed that the microvascular density was significantly decreased in *+/hIC1* placentas among males (Figure 3H and Supplemental Figure 1D). Although previous studies reported that *Igf2*-null mice had lower placental glycogen concentration (Lopez et al., 1996) and *H19* deletion led to increased placental glycogen storage (Esquiliano et al., 2009), Periodic acid-Schiff (PAS) staining on

167 *+/hIC1* placentas showed that the glycogen content is not significantly different between wild-type and
168 *+/hIC1* placentas (Supplemental Figure 1E). The reduced labyrinth layer and defective microvascular
169 expansion likely compromised the ability of *+/hIC1* placentas to supply nutrients and oxygen to the fetus.
170 These results support the hypothesis that the abnormal growth of *+/hIC1* embryos may be explained by
171 failure in multiple organs, especially the heart and placenta, which are developmentally linked (Barak et
172 al., 2019).

173 Additionally, we examined expression of the *H19*-derived miR-675 in *+/hIC1* placentas to
174 determine if the level of miR-675 is correlated with changes in *H19* and *Igf2* expression. This analysis
175 was conducted at E15.5 when cardiac and placental defects were already observed in *+/hIC1* embryos
176 (Supplemental Figure 1A, 1C and Supplemental Figure 2). Despite increased *H19* expression and *Igf2*
177 depletion (Hur et al., 2016), miR-675 was not significantly increased in *+/hIC1* placentas compared to the
178 wild-type (Supplemental Figure 1F). Thus, we conclude that the placental phenotypes observed in *+/hIC1*
179 mice are solely attributable to the increased *H19* lncRNA, irrespective of miR-675. Another possibility is
180 that the disproportionate *H19* overexpression in the labyrinth layer at E17.5 (Figure 3D) was also present
181 at E15.5 because growth suppression was more severe in labyrinth than in junctional zone in E15.5
182 (Supplemental Figure 1C) and in E17.5 placenta (Figure 3C). This would have made it difficult to detect a
183 substantial difference in miR-675 expression in the whole placenta.

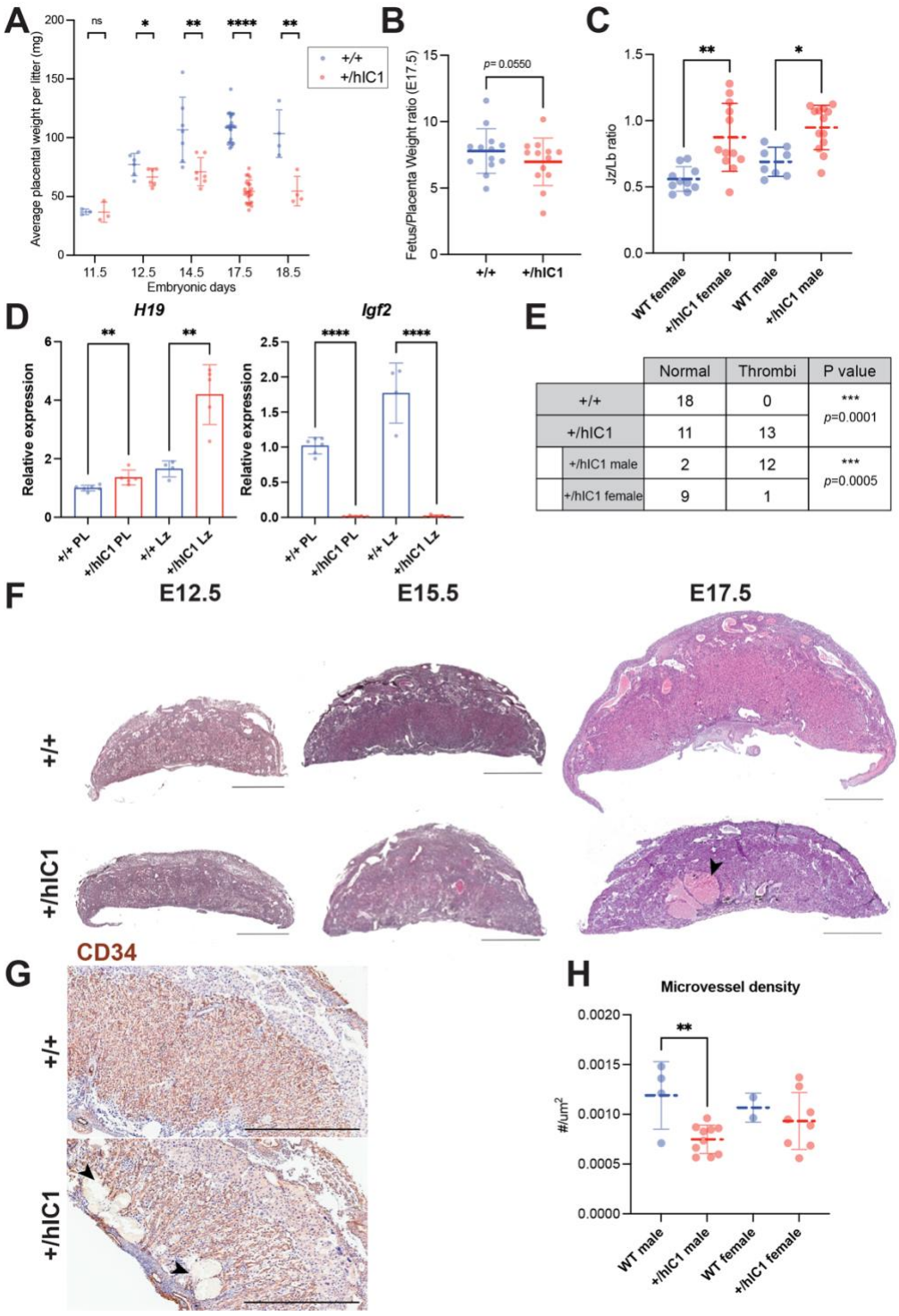

	Normal	Thrombi	P value
+/+	18	0	*** p=0.0001
+/hIC1	11	13	
+/hIC1 male	2	12	*** p=0.0005
+/hIC1 female	9	1	

184

Figure 3. Placental defects of *+/hIC1* embryos.

(A) Placental weight of the wild-type (blue) and *+/hIC1* (red) samples at E11.5, E12.5, E14.5, E17.5 and E18.5 (mean ± SD). Each data point represents an average weight of each genotype from one litter. 3 litters for E11.5, 6 litters for E12.5, 7 litters for E14.5, 22 litters for E17.5, 4 litters for E18.5 are presented. (B) Fetal to placental weight ratios in E17.5 wild-type and *+/hIC1* samples (mean ± SD).

Each data point represents the average F/P ratio of each genotype from one litter. 13 litters are presented. (C) Junctional zone (Jz) to labyrinth (Lb) ratio in E17.5 wild-type and *+/hIC1* placentas (mean ± SD). (D) Relative total expression of *H19* and *Igf2* in E17.5 wild-type and *+/hIC1* placentas and labyrinth samples (mean ± SD). (E) Number of wild-type, male and female *+/hIC1* placentas with thrombi observed. (F) Representative cross-sections of E12.5, E15.5 and E17.5 wild-type and *+/hIC1* placentas stained with hematoxylin and eosin. All depicted E12.5, E15.5 placentas are female. The E17.5 wild-type placenta is female and +/*hIC1* placenta is male. Black arrowhead indicates a large thrombus formed in the *+/hIC1* labyrinth. Scale bars = 1mm. (G) Representative images of CD34 immunostaining counterstained with hematoxylin on E17.5 wild-type female and *+/hIC1* male placental sections. Black arrowheads indicate thrombi in the *+/hIC1* labyrinth. Scale bars = 1mm. (H) Quantification of the microvessel density in E17.5 wild-type and *+/hIC1* placentas. 4 wild-type male, 10 *+/hIC1* male, 2 wild-type female, 8 *+/hIC1* female placentas from 6 litters were quantified. (C, D, H) Each data point represents an individual conceptus from different litters. Statistics used are (A, B) multiple paired t-test, (C) one-way ANOVA with Tukey's multiple comparisons test, (D, H) multiple unpaired t-test, (E) Fisher's exact test. *P < 0.05, **P < 0.01, ***P < 0.001, ****P < 0.0001, ns = not

Normalizing *H19* expression partially rescues paternal *hIC1* defects

It has been previously reported that *Igf2* null mice are viable (DeChiara et al., 1991). Thus, we hypothesize that *H19* overexpression combined with a loss of *Igf2* expression is the molecular contributor to the lethality of paternal *hIC1* transmission. To examine if reduced *H19* expression would rescue the paternal *hIC1* transmission phenotypes, we generated a mouse model with deletion of the *H19* transcription unit [$H19^{\Delta 2.8kb\text{-}H19}$; shortened as *⊿H19*] (Figure 1B, Supplemental Figure 3A and B). Consistent with previous reports, maternal deletion of *H19* [*⊿H19/+*] led to an absence of *H19* expression and tissue-specific minimal activation of maternal *Igf2* (Supplemental Figure 3C). These mice are viable and fertile, regardless of whether the deletion is maternally or paternally transmitted, although maternal transmission is associated with increased fetal weight from E14.5 and onwards (Supplemental Figure 3D).

Heterozygous *⊿H19* females were mated with heterozygous *hIC1* males to generate *⊿H19/hIC1* embryos. These embryos were expected to have lower *H19* expression compared to *+/hIC1* embryos, as the maternal *H19* expression was silenced (Figure 4A). Among four possible genotypes from this

breeding, *+/hIC1* embryos constituted approximately 15% per litter at E17.5, as opposed to the expected Mendelian ratio of 25%. In contrast, *⊿H19/hIC1* embryos comprised approximately 30% per litter at E17.5, indicating partial rescue of the resorption frequency by maternal *H19* deletion (Figure 4B and Supplemental Figure 4A). However, *⊿H19/hIC1* embryos still exhibited perinatal lethality, with no live pups observed on the day of birth. With respect to growth restriction, the maternal *⊿H19* allele partially rescued the phenotype. At E11.5, *⊿H19/hIC1* fetal weight was not significantly different from wild-type littermates (Figure 4C). However, at late gestation (E17.5), although *⊿H19/hIC1* fetuses had a significant increase in fetal weight compared to the *+/hIC1* fetuses, *⊿H19/hIC1* fetuses remained significantly smaller compared to wild-type. As perinatal lethality was still observed, conceptuses were analyzed histologically to characterize their developmental defects. The AV cushion defect persisted in all examined E13.5 *⊿H19/hIC1* embryos, and 50% of the examined E17.5 *⊿H19/hIC1* hearts showed either perimembranous or muscular VSDs (Figure 4D). Thrombi were still present in approximately 50% of *⊿H19/hIC1* placentas (Figure 4E and Supplemental Figure 4D), and placental weight remained significantly lower compared to wild-type littermates (Supplemental Figure 4B). Of note, none of these histological defects were observed in *⊿H19/+* embryonic hearts and placentas (see Figure 4D for example; 3 *⊿H19/+* hearts each from E13.5, E15.5 and E17.5 concepti, and 20 E17.5 *⊿H19/+* placentas were examined). E17.5 *⊿H19/hIC1* tissues demonstrated wild-type levels of *H19* expression, while the *Igf2* expression remained markedly lower than wild-type (Figure 4F and Supplemental Figure 4C). From these results, we conclude that restoring *H19* expression is not sufficient to rescue completely the lethality and developmental defects upon paternal transmission of *hIC1*. Thus, phenotypes are likely caused by abnormal expression of both *H19* and *Igf2*.

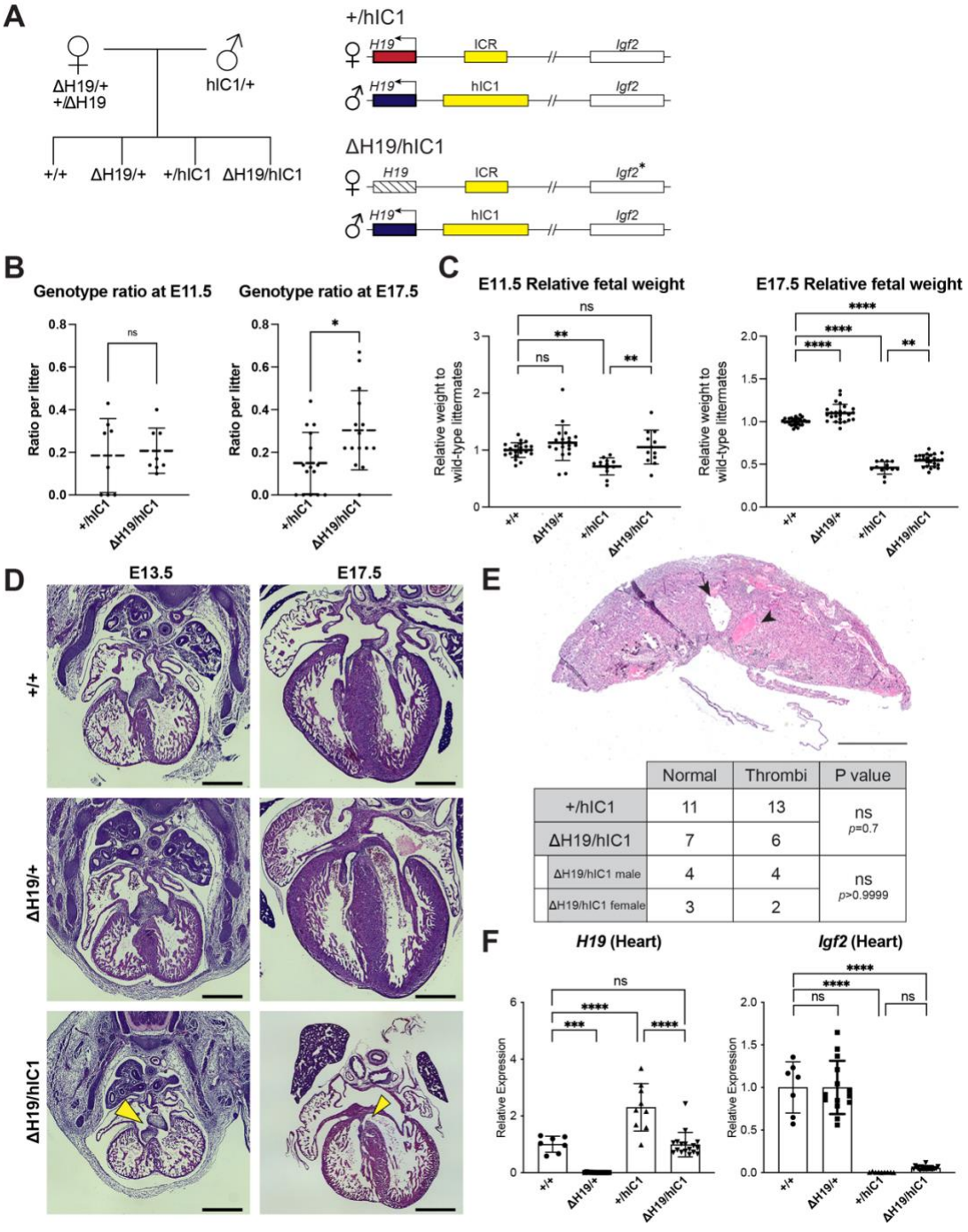

221

Figure 4. Normalizing *H19* expression through the maternal deletion of *H19*.

(A) A schematic representation of the rescue breeding between *⊿H19* heterozygous female and *hIC1/+* male mice. *⊿H19/hIC1* embryos are expected to express *H19* only from the paternal allele, and maternally express *Igf2* in a tissue-specific manner. (B) Ratio of *+/hIC1* and *⊿H19/hIC1* embryos observed in E11.5 and E17.5 litters (mean ± SD). 8 E11.5 litters and 15 E17.5 litters with litter size larger than 5 pups were examined. Each data point represents one litter. (C) Relative fetal weights of wild-type, *⊿H19/+, +/hIC1* and *⊿H19/hIC1* embryos at E11.5 and E17.5, normalized to the average

body weight of the wild-type littermates (mean ± SD). (D) Representative cross-sections of wild-type, *⊿H19/+* and *⊿H19/hIC1* embryonic hearts at E13.5 and E17.5, stained with hematoxylin and eosin. Note the cushion defect at E13.5 and the VSD at E17.5 in *⊿H19/hIC1* hearts (yellow arrows). All E13.5 samples and E17.5 wild-type sample are male, E17.5 *⊿H19/+* and *⊿H19/hIC1* samples are female. Scale bars = 500 µm. (E) (Top) Representative cross-section of E17.5 *⊿H19/hIC1* male placenta stained with hematoxylin and eosin. Black arrowheads indicate thrombi. Scale bar = 1mm. (Bottom) Number of the wild-type, male and female *+/hIC1* placentas with thrombi observed. (F) Relative total expression of *H19* and *Igf2* in E17.5 wild-type, *⊿H19/+, +/hIC1* and *⊿H19/hIC1* hearts (mean ± SD). (C, F) Each data point represents an individual conceptus from different litters. Statistics used are (B, C, F) one-way ANOVA with Tukey's multiple comparisons test and (E) Fisher's exact test. **P* < 0.05, ***P* < 0.01, ****P* < 0.001, *****P* < 0.0001, ns = not significant.

Paternal *hIC1* defects are rescued by deletion of the maternal *H19/Igf2* ICR

Finally, we utilized a previously published mouse model with a 3.8-kb deletion spanning the *H19/Igf2* ICR [$H19^{\Delta 3.8kb\text{-}5'H19}$; shortened as *⊿3.8*] to modulate both *H19* and *Igf2* expression (Thorvaldsen et al., 2002, 2006). Absence of the maternal *H19/Igf2* ICR activates the maternal *Igf2* allele and reduces *H19* expression. Thus, *Igf2* expression from the maternal allele in *⊿3.8/hIC1* embryos was expected to restore *Igf2* levels (Figure 5A).

Crosses between heterozygous *⊿3.8* females and heterozygous *hIC1* males produced the expected Mendelian ratio of offspring with *⊿3.8/hIC1* mice appearing fully viable. Both fetal and placental weights were not significantly different between *⊿3.8/hIC1* and wild-type concepti at E17.5 (Figure 5B and Supplemental Figure 5A), demonstrating full rescue of the lethality and growth restriction. However, a subset of *⊿3.8/+* and *⊿3.8/hIC1* embryonic hearts (3 out of 6 *⊿3.8/+* hearts and 2 out of 5 *⊿3.8/hIC1* hearts) had VSDs, although the lesions in the IVS were smaller than those found in *+/hIC1* hearts (Figure 5C). While *Igf2* expression in the E17.5 *⊿3.8/hIC1* hearts was restored to wild-type levels, normalization of *H19* expression varied among embryos. Although not statistically significant in heart, *⊿3.8/hIC1* embryos tended to have higher *H19* expression compared to the wild-type littermates (Figure 5D and Supplemental Figure 5B). These results suggest that the physiological levels of *H19* and

Igf2 expression are critical for normal cardiac development, and the variability in *H19* rescue could help to explain the varying penetrance of the cardiac phenotype. No thrombi were detected in the *⊿3.8/hIC1* placentas, and the placental morphology was normal with the junctional to labyrinth zone ratio not significantly different compared to wild-type (Supplemental Figure 5C). In sum, restoring both *H19* and *Igf2* to near wild-type levels was necessary for the full rescue of the most severe pathologies of paternal *hIC1* transmission.

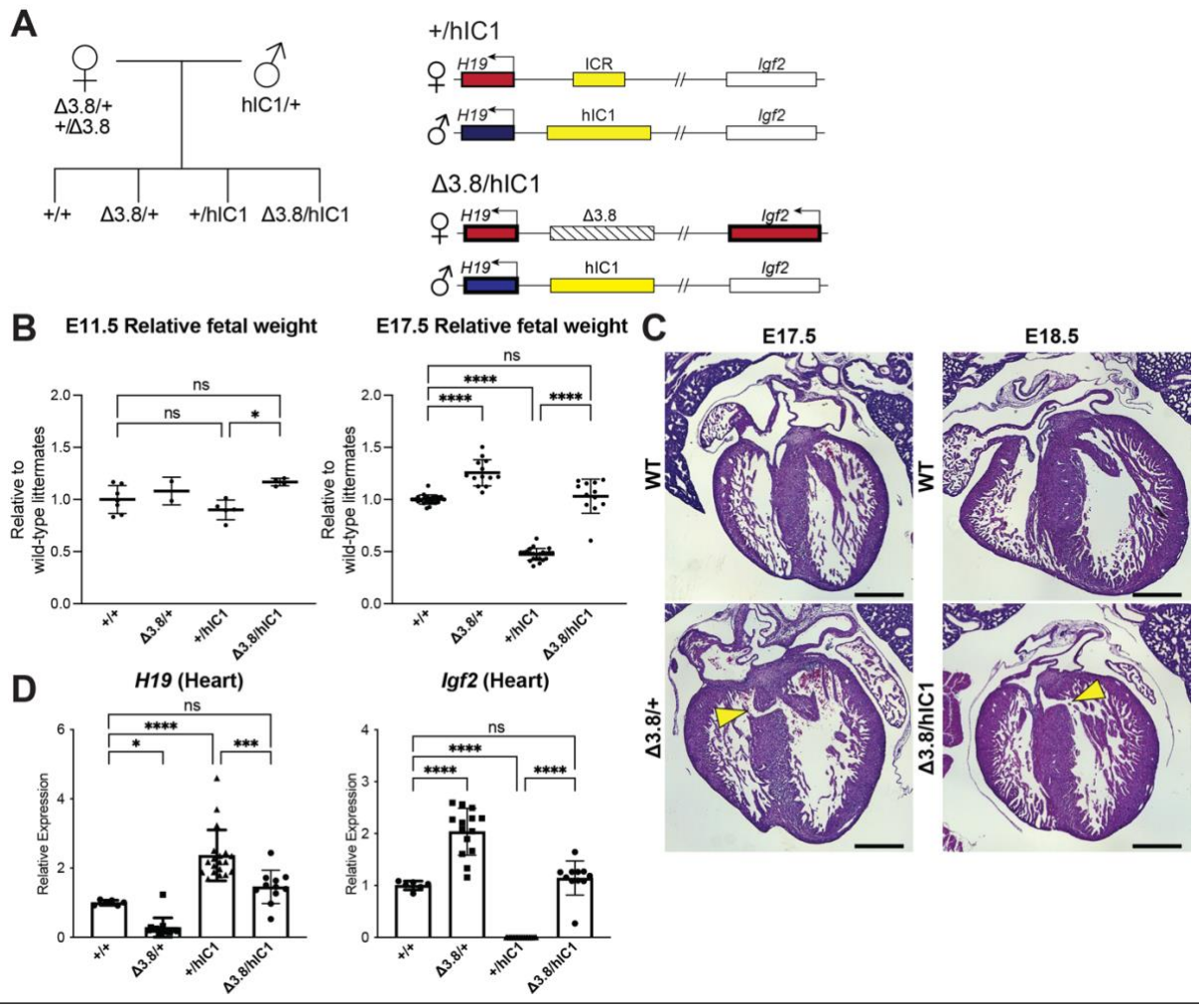

245

Figure 5. Restoring *H19* and *Igf2* expression utilizing maternal *H19/Igf2* ICR deletion.
(A) A schematic representation of the offspring produced when *⊿3.8* heterozygous female and *hIC1/+* male mice are mated is depicted. *⊿3.8/hIC1* embryos are expected to show activation of maternal *Igf2* expression as well as paternal *H19* expression. (B) Relative fetal weights of wild-type, *⊿3.8/+, +/hIC1,* and *⊿3.8/hIC1* embryos at E11.5 and E17.5, normalized to the average body weight of wild-type littermates (mean ± SD). 2 E11.5 and 10 E17.5 litters are presented. (C) Representative cross-sections of E17.5 *⊿3.8/+* and E18.5 *⊿3.8/hIC1* embryonic hearts with VSDs (yellow arrows), stained with hematoxylin and eosin. Sections from wild-type littermates are shown together for comparison. The E17.5 wild-type sample is male, the rest are female. Scale bars = 500 μm. (D) Relative total expression of *H19* and *Igf2* in E17.5 wild-type, *⊿3.8/+, +/hIC1,* and *⊿3.8/hIC1* hearts (mean ± SD). (B, D) Each data point represents an individual conceptus from different litters. One-way ANOVA with Tukey's multiple comparisons test was used with **P* < 0.05, ****P* < 0.001, *****P* < 0.0001 and ns = not significant.

Transcriptomic analysis of cardiac endothelial cells with various *H19/Igf2* expression

Severe cardiac phenotypes associated with paternal *hIC1* transmission prompted us to question the mechanism of how dysregulated *H19/Igf2* causes such developmental defects. The paternal *hIC1*-associated cardiac phenotypes were observed as early as E12.5 when AV cushion fusion is delayed in developing hearts (Figure 2B), making E12.5 an optimal time point to identify the key pathways of valve development and cardiac septation that are disrupted by *H19/Igf2* dysregulation. Endothelial and endothelial-derived cells comprise the majority population in the AV cushion and majority non-myocyte population of the ventricular septum at E12.5 (Von Gise & Pu, 2012). Moreover, both *H19* and *Igf2* are strongly expressed in the endocardial layer of developing heart (García-Padilla et al., 2019). Therefore, transcriptomic analysis was performed on cardiac endothelial cells of each mutant.

CD31+ cardiac endothelial cells from E12.5 wild-type, *+/hIC1*, *⊿H19/+*, *⊿H19/hIC1*, *⊿3.8/+*, and *⊿3.8/hIC1* embryos were collected for RNA sequencing. First, we confirmed that these 6 groups show gradual alteration of *H19*/*Igf2* expression (Figure 6A), which enabled us to generate multiple comparisons relative to *H19* and *Igf2* levels and potentially enabling attribution of phenotypes to *H19* or *Igf2*. Notably, *H19*/*Igf2* expression was indistinguishable in the wild-type and *⊿3.8/hIC1* samples. Additionally, there were no sex-specific differences in *H19*/*Igf2* expression across all the groups.

To elucidate candidate genes and cellular processes in conferring the paternal *hIC1*-specific cardiac phenotypes, we compared *+/hIC1* and wild-type samples. This comparison resulted in 224 significant differentially expressed genes (DEGs) (Figure 6B, left). Gene ontology (GO) analysis revealed that pathways related to proliferation and remodeling of endothelial and epithelial cells are enriched in these DEGs (Figure 6B, right) (Mi et al., 2019). Notably, genes involved in extracellular matrix (ECM) and specifically, collagen matrix production, were differentially enriched in E12.5 *+/hIC1* samples; consistent with increased collagen in the E17.5 *+/hIC1* hearts, as confirmed through immunofluorescence staining (Figure 6C, Supplemental Figure 6A and B). Thus, differential gene expression in the presence of paternal *hIC1* was evidenced by E12.5 and correlated with histological consequences persisting through gestation.

Because cardiac phenotypes were indistinguishable between males and females, we next used same-sex comparisons between *+/hIC1* and wild-type to identify the *hIC1*-specific DEGs that are significant in both males and females (Figure 6D, left and Supplemental Figure 6C). The 25 genes that overlapped between male and female *+/hIC1*-specific DEGs included *Col14a1,* which was upregulated in *+/hIC1*, emphasizing the importance of collagen-related ECM in *hIC1*-associated cardiac defects. The expression pattern of these 25 genes across all samples clustered *+/hIC1* and *⊿H19/hIC1*, the two groups with the most severe cardiac defects and perinatal lethality (Figure 6D, right). Although the number of *+/hIC1*-specific DEGs largely differed between males and females, there was no sex-specific bias on the X chromosome (Supplemental Figure 6D).

To separate the effect of *Igf2* depletion from that of *H19* overexpression, we utilized *⊿H19/hIC1* samples. Consistent with previous observations from E17.5 hearts (Figure 4F), *⊿H19/hIC1* endothelial cells exhibited low *Igf2,* but *H19* expression was not significantly different from wild-type (Supplemental Figure 7A). Thus, *⊿H19/hIC1* samples were compared to *+/hIC1* to clarify the sole effect of *H19* overexpression. Here, 46 DEGs were identified (Supplemental Figure 7B), which were enriched in vascular endothelial cell proliferation pathways (Supplemental Figure 7C). Surprisingly, although physiologically similar to *+/hIC1*, the *⊿H19/hIC1* transcriptome was quite different from that of *+/hIC1*. Compared to wild-type, *⊿H19/hIC1* only had 23 DEGs (Supplemental Figure 7A), in contrast to *+/hIC1* showing more than 200 DEGs compared to wild-type (Figure 6B, left). This result underscores the overwhelming effect of increased *H19* in transcriptomic regulation.

To identify the genes whose expression is solely affected by *H19,* we compared *+/hIC1,* *⊿H19/hIC1*, and *⊿H19/+* endothelial cells. Among 224 genes that are differentially expressed in *+/hIC1* endothelial cells relative to wild-type, 15 genes are also differentially expressed in *⊿H19/hIC1* samples, suggesting that these 15 genes were affected by the loss of *Igf2* rather than increased *H19.* Among the remaining 209 DEGs that are not altered in *⊿H19/hIC1* samples, only *Fgf10* and *H19* were also differentially expressed in *⊿H19/+* endothelial cells compared to wild-type. *Fgf10,* a key regulator of

297 cardiac fibroblast development, mediates communication between cardiac progenitor cells and regulates
298 cardiac myocyte proliferation (Hubert et al., 2018; Vega-Hernández et al., 2011). Consistently, *Fgf10* null
299 mouse embryos showed abnormal cardiac morphology with reduced heart size and thinned ventricular
300 wall (Rochais et al., 2014; Vega-Hernández et al., 2011). In our samples, *Fgf10* is upregulated when *H19*
301 is deleted and downregulated upon *H19* overexpression, linking *H19* and *Fgf10* closely in the context of
302 cardiac development. Additionally, Gene Set Enrichment Analysis (GSEA) revealed that the set of
303 imprinted genes (BRIDEAU_IMPRINTED_GENES) including *Cdkn1c*, *Dlk1* and *Gatm* was
304 differentially enriched in *+/hIC1* samples (Supplemental Figure 8A) (Mootha et al., 2003; Subramanian et
305 al., 2005). The same set of genes was also differentially enriched in *⊿H19/+* samples (Supplemental
306 Figure 8B), but not *⊿H19/hIC1* (Supplemental Figure 8C), underscoring a role for *H19* as a master
307 regulator of the imprinted gene network (IGN) (Gabory et al., 2010).
308 We then analyzed *⊿3.8/hIC1* samples to identify cellular processes that are required to rescue the
309 paternal *hIC1*-associated lethality, as *⊿3.8/hIC1* mice are fully viable with occasionally observed VSD.
310 *⊿3.8/hIC1* had only two DEGs compared to wild-type (Figure 6E). However, the *Shh* expression was
311 only detected in two wild-type samples, suggesting that *Shh* did not have significant affect in the
312 development of our wild-type and *⊿3.8/hIC1* cardiac endothelial cells at this stage. In contrast, 487 genes
313 were differentially expressed in *⊿3.8/hIC1* compared to *+/hIC1* (Supplemental Figure 9A). Within these
314 DEGs, we wanted to clarify the genes that were likely involved in restoring viability. The 487 DEGs
315 between *+/hIC1* and *⊿3.8/hIC1* were compared to the DEGs between *+/hIC1* and wild-type to filter
316 genes that are commonly affected in both comparisons (Figure 6F, left). GO analysis showed that the 116
317 overlapping genes are associated with endothelial/epithelial cell proliferation and remodeling
318 (Supplemental Figure 9B), emphasizing the importance of the proper regulation of these pathways in the
319 rescued viability of *⊿3.8/hIC1* embryos. The expression pattern of these 116 genes clustered *+/hIC1* and
320 *⊿H19/hIC1*, implicating these genes in the perinatal lethality characteristic of these two groups (Figure
321 6F, right).

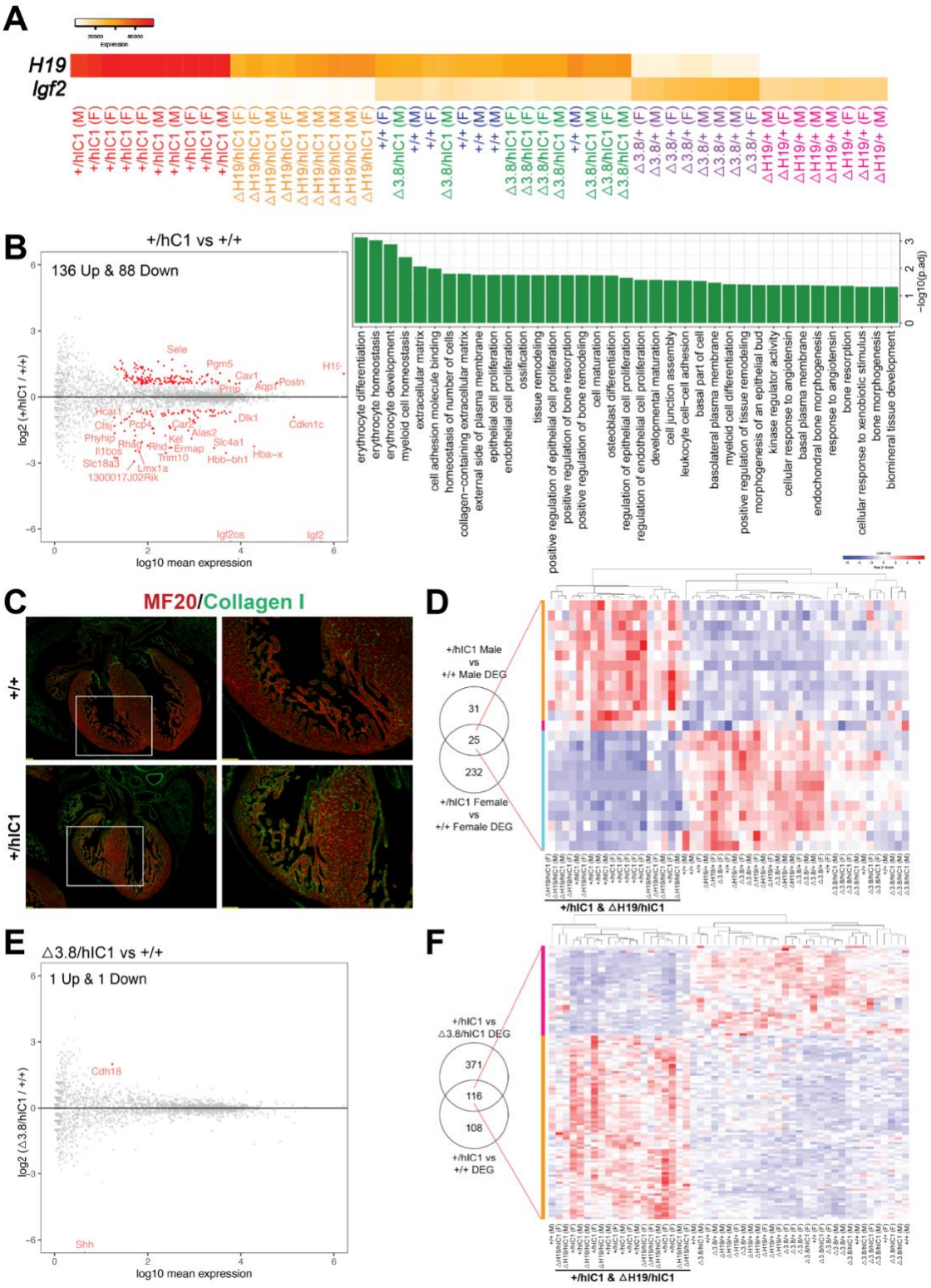

Figure 6. Transcriptomic analysis of E12.5 cardiac endothelial cells from wild-type and mutant embryos.

(A) A gradient *H19* and *Igf2* expression levels are depicted in E12.5 wild-type, *+/hIC1, ⊿H19/+, ⊿H19/hIC1, ⊿3.8/+* and *⊿3.8/hIC1* cardiac endothelial cells. M: Male, F: Female. (B) (Left) Comparison between *+/hIC1* and the wild-type samples with a volcano plot shows 224 DEGs between *+/hIC1* and the wild-type samples. (Right) GO pathways that are enriched for the 224 DEGs. (C) Immunofluorescence staining for MF20 (red) and collagen (green) on E17.5 wild-type and *+/hIC1* hearts. Images on the right are enlarged from the boxed area of images on the left. Scale bars = 100 μm. (D) Expression pattern of 25 genes that are differentially expressed in both male and female *+/hIC1* samples is compared to wild-type. (E) A volcano plot represents 2 DEGs between *⊿3.8/hIC1* and the wild-type samples. (F) Expression pattern of 116 genes that are commonly differentially expressed in *+/hIC1* compared to the wild-type and *⊿3.8/hIC1* samples.

Discussion

In this study, we report that the overexpression of *H19* combined with *Igf2* depletion leads to severe morphological defects in the heart and placenta, which are likely to be involved with the perinatal lethality and restricted growth of SRS mouse models. Genetically correcting *H19* was not sufficient to fully rescue the developmental defects, indicating that the SRS-like phenotypes of paternal *hIC1* transmission are not solely attributable to *H19* overexpression. Unexpectedly, although moderately adjusting both *H19* and *Igf2* rescued the lethality, septal defects persisted in some of the *⊿3.8/hIC1* embryos, suggesting that cardiac development is extremely sensitive to the dosage of *H19* and *Igf2*. Our transcriptomic profiling of cardiac endothelial cells with various levels of *H19* and *Igf2* expression uncovers critical pathways driven by *H19* and *Igf2* that are important for cardiac structure formation. The result suggests that the regulation of ECM and proliferation of endothelial cells are tightly regulated by *H19* and *Igf2*, and potentially responsible for the paternal *hIC1*-associated cardiac defects.

The function of *H19* in cardiac development is understudied even though the expression of *H19* is robust in the developing endocardium and epicardium throughout gestation (García-Padilla et al., 2019). Abnormal *H19/Igf2* expression in *+/hIC1* hearts disrupted AV cushion fusion, ventricular septation and valve formation processes with variable penetrance. These events require properly established ECM, which accommodates endothelial-mesenchymal transition, cell proliferation, and cell-cell adhesion in

342 developing hearts (Kruithof et al., 2007; Sullivan & Black, 2013; Von Gise & Pu, 2012). In adult murine
343 hearts, where *H19* has been well implicated in cardiac fibrosis and remodeling (Greco et al., 2016; Hobuß
344 et al., 2020; Lee et al., 2011; Wang et al., 2021), *H19* overexpression led to increased ECM and fibrosis
345 markers after myocardial injury, while deleting *H19* resulted in downregulated ECM genes (Choong et
346 al., 2019). In our *+/hIC1* endothelial cells, the expression of several key ECM genes such as *Periostin*
347 (*Postn*) (Snider, 2009; Sullivan, 2013), *Col14a1*, and *Adamts17* (Hubmacher, 2015) was significantly
348 upregulated compared to wild-type cells. Combined with increased collagen in E17.5 *+/hIC1* hearts
349 (Figure 6C), we hypothesize that failing to establish proper ECM contributes significantly to the *+/hIC1*-
350 associated cardiac defects during development. Additionally, regulators of cell proliferation, including
351 *E2f5, Trabd2b,* and *Septin4,* and genes associated with inflammation such as *Sele* and *Cd200* were also
352 differentially expressed in *+/hIC1* samples. Overall, this work provides some hints regarding the potential
353 mechanism underlying how increased *H19* expression disrupts normal cardiac development.
354 In contrast to the less well understood role for *H19*, *Igf2* is the main growth factor in the
355 developing ventricular wall. Similar to *H19, Igf2* is highly expressed in the developing cardiac
356 endocardium and epicardium from early gestation (Shen et al., 2015) before ventricular septation is
357 completed (Savolainen et al., 2009). Deletion of *Igf2* and its receptors caused decreased cardiomyocyte
358 proliferation and ventricular hypoplasia, suggesting that *Igf2* is the major regulator of ventricular wall
359 thickening (Li et al., 2011; Shen et al., 2015). Additionally, the interventricular septum is comprised of
360 both mesenchymal and muscular components (Penny & Vick, 2011; Spicer et al., 2014), and a reduction
361 in cardiomyocyte proliferation can lead to VSD (Snider & Conway, 2011). Thus, the lack of *Igf2*, a
362 growth promoter for cardiomyocytes, could have contributed to the septal defects observed in *+/hIC1* and
363 *⊿H19/hIC1* hearts. However, the thinned myocardium in *Igf2* knockout mouse embryos was resolved by
364 birth, resulting in normal cardiac morphology in neonates (Shen et al., 2020). In contrast, ventricular wall
365 thinning and septal defects in *+/hIC1* and *⊿H19/hIC1* hearts were aggravated towards the end of
366 gestation, indicating that these phenotypes are not exclusively attributable to the loss of *Igf2* expression.

Recovery of *Igf2* expression in *⊿3.8/hIC1* hearts rescued ventricular hypoplasia, consistent with previous findings (Li et al., 2011; Shen et al., 2015). In contrast, septal defects persist in some *⊿3.8/+* and *⊿3.8/hIC1* embryos. Because *Igf2* expression varied substantially among *⊿3.8/+* and *⊿3.8/hIC1* hearts (Figure 5D), we hypothesize that the varying penetrance of septal defects in these hearts reflects the range of *H19/Igf2* levels. The only upregulated gene in *⊿3.8/hIC1* endothelial cells compared to wild-type was *Cadherin 18 (Cdh18)* (Figure 6E), which was also upregulated in *⊿3.8/+* samples compared to wild-type (Supplemental Figure 9C) and clinically reported to be mutated in CHDs including VSD (Chen et al., 2018; Soemedi et al., 2012). Although we and others showed that restoring *Igf2* successfully rescues the growth restriction in SRS-like mouse models (Han et al., 2010; Liao et al., 2021), septal defects caused by *H19* and *Igf2* dysregulation are reported for the first time in this study. Our data provide evidence that ventricular septation may be regulated separately from the ventricular wall thickening, and that both events are extremely sensitive to the level of *H19* and *Igf2* expression. In humans, VSDs were found in SRS patients with IC1 hypomethylation (Ghanim et al., 2013) and a patient carrying chromosomal gain of chr11p15 (Serra et al., 2012). Thus, the VSD observed in our mouse models nicely models the SRS-associated CHD in human patients. It should be noted, however, that mice are often more susceptible to VSDs than humans. Mice with VSDs show a higher neonatal mortality rate, possibly due to the higher heart rates and relatively larger size of VSD lesions (Snider & Conway, 2011). Additionally, cardiac defects that are lethal in mice can lead to spontaneous miscarriages in humans due to longer human gestation, making it difficult to observe human infants with similar defects.

Linked through fetoplacental blood circulation, the heart and placenta are closely connected under the cardiac-placental axis, which is crucial for fetal growth and viability (Barak et al., 2019; Maslen, 2018). Both organs are responsible for supplying nutrients and oxygen for developing fetuses, and placental and cardiac defects are often coupled in mouse models (Perez-Garcia et al., 2018) and humans (Matthiesen et al., 2016; Rychik et al., 2018). Placental maintenance of a normoxic fetal environment is vital for cardiac morphogenesis, and hypoxia can lead to severe defects emerging especially in cushions and septa (Dor et al., 2001). Epicardial *Igf2* expression in developing ventricles is

induced by a normoxic environment that is dependent on the placental function (Shen et al., 2015), while *H19* is upregulated under hypoxic conditions in mouse cardiomyocytes (Choong et al., 2019). This suggests that *H19* and *Igf2* are important mediators of the interaction between heart and placenta. Consistent with previous reports, gene sets of which expression is altered under hypoxic conditions (HALLMARK_HYPOXIA, GROSS_HYPOXIA_VIA_HIF1A_DN) are differentially enriched in our *+/hIC1* endothelial cells compared to wild-type (Supplemental Figure 10). As the heart and placenta are responsible for meeting the fetal demand for nutrients and oxygen, the malfunction of these two organs would severely constrain embryonic growth. Therefore, the precise role of *H19* and *Igf2* in cardiac-placental communication needs to be clarified to understand how the SRS-related growth restriction is induced by IC1 hypomethylation.

The labyrinth, where *+/hIC1* placentas show abnormal vasculature morphology and thrombosis, serves as a prime location for maternal-fetal blood exchange (Woods et al., 2018). Placental thrombosis can be caused by defective labyrinth integrity, and diminished labyrinth function could limit the nutritional and oxygen supply for a fetus, which can, in turn, lead to hypoxia and growth restriction. Both *H19* and *Igf2* are highly expressed in fetoplacental endothelial cells in the labyrinth (Aykroyd et al., 2022; Sandovici et al., 2022). Genetically depleting *Igf2* expression in the epiblast lineage led to decreased labyrinth size and caused the formation of thrombi in the labyrinth, although the lesions were smaller in size than those observed in *+/hIC1* placentas (Sandovici et al., 2022). Depletion of the placental-specific *Igf2* transcript in mice resulted in a smaller labyrinth and fetal growth restriction (Constância et al., 2002; Sibley et al., 2004), although these mice showed an increased fetal to placental weight ratio, which was decreased in *+/hIC1* mice. This contrasting result could be explained by the effect of the increased *H19* expression in *+/hIC1* mice. *H19* regulates vascular endothelial growth factor (VEGF) in human endothelial cells *in vitro* (Conigliaro et al., 2015), which is involved in placental angiogenesis, specifically for the branching of fetoplacental vessels beginning at mid-gestation (Woods et al., 2018). Additionally, *H19* is highly expressed in trophoblasts (Marsh & Blelloch, 2020; Poirier et al., 1991), and disrupted trophoblast development leads to defective vascular branching in the labyrinth and restricted

fetal growth (Ueno et al., 2013). Thus, it is possible that the morphological anomalies observed in the *+/hIC1* placenta are exaggerated by abnormal *H19* expression in trophoblasts. Transcriptomic analysis of fetoplacental endothelial cells from our mouse models would help us understand the role of *H19/Igf2* in placental development. Moreover, generating a tissue-specific *hIC1* mouse model, if possible, would allow us to determine the causal relationship between cardiac and placental phenotypes.

In summary, we provide evidence that the proper dosage of *H19* and *Igf2* is essential for normal cardiac and placental development. Investigation of the role of *H19* and *Igf2* in the cardiac-placental axis will enable a better understanding of how paternal *hIC1* transmission leads to the SRS-like growth restriction and perinatal lethality. As many patients with SRS exhibit DNA methylation mosaicism, the distribution of the epimutation, which reflects the severity of patient symptoms, varies. This work provides insight into identifying organs that are most sensitive to *H19* and *Igf2* dysregulation, which would allow us to develop early intervention methods for critical SRS pathologies with such variabilities.

Materials and Methods

Animal studies. All studies were approved by the Institutional Animal Care and Use Committee (IACUC) at the University of Pennsylvania. *hIC1* (Hur et al., 2016) and *⊿3.8* (Thorvaldsen et al., 2002, 2006) mouse models were previously described. Generation of *⊿H19* line is described in Supplemental Information. Timed breeding was performed as previously described (SanMiguel et al., 2018). Vaginal sperm plugs were checked to calculate the age, and the day of the plug was marked as E0.5. Visual staging confirmed the embryonic days at the time of dissection. All mice were maintained on C57BL/6 background for more than 10 generations if not noted otherwise. Genotyping was performed as described in Supplemental Information.

Gene Expression Analysis. Mouse tissues were ground using pestles, syringes and needles in either TRIzol (Thermo Fisher scientific, Waltham, MA) or RLP buffer included in RNeasy Mini kit (Qiagen, Hilden, Germany). RNA was isolated according to the manufacturer's instructions. cDNA synthesis, qRT-PCR, and allele-specific expression analysis was performed as previously described (Hur et al.,

2016). Primers and PCR conditions are listed in Supplemental Table 1. RNA Sequencing library preparation and analysis are described in Supplemental Information. Total expression levels of miR-675-3p and miR-675-5p were determined relative to snoRNA202 by using a separate RT kit (TaqMan MicroRNA Reverse Transcription Kit, Thermo Fisher Scientific), qRT-PCR primers (Assay Id 001232, 001941, 001940, Thermo Fisher Scientific), and a PCR master mix (TaqMan Universal PCR Master Mix, catalog number 4304437, Thermo Fisher Scientific) according to manufacturer's protocol.

Histological analysis. Mouse heart and placenta samples were collected in cold PBS, fixed overnight in 4% paraformaldehyde or 10% phosphate-buffered formalin and processed through ethanol dehydration. Tissues were paraffin-embedded and sectioned for further staining analysis. Hematoxylin and eosin staining was performed using a standard protocol. Immunohistochemistry for MF20 (Developmental Studies Hybridoma Bank, Iowa City, IA) and Collagen I (cat# ab34710, Abcam, Cambridge, UK) was performed with primary antibody incubations overnight at 4°C. Prior to antibody incubation, antigen retrieval with citrate buffer was performed, followed by a 1 hour block in 10% normal serum. DAPI (cat#32670-5MG-F, Sigma-Aldrich, St. Louis, MO) was used as a counter stain, and slides were mounted with VECTASHILD (Vector, Burlingame, CA). Images were taken on a Leica DMi8S widefield microscope. Placental CD34 staining and Periodic acid-Schiff (PAS) staining was previously described (Vrooman et al., 2020). The thickness of ventricular wall was measured on hematoxylin-eosin-stained heart sections using Adobe Photoshop. A minimum of 3 distinct sections were quantified for each mouse of each genotype in a blinded manner. Placental Jz/Lb ratio was measured using FIJI (ImageJ v2.0.0, Schindelin et al., 2012) in a blinded manner. CD34 stained placental sections were digitally scanned using Aperio VERSA 200 platform in Comparative Pathology Core (CPC) at School of Veterinary Medicine at the University of Pennsylvania. Images were analyzed via Aperio Microvessel Analysis algorithm as previously described (Vrooman et al., 2020).

Statistical Analysis. Differences between two groups were evaluated using Student's t-test. For three or more groups, ordinary one-way analysis of variance (ANOVA), followed up with Tukey's multiple comparisons test, was used. Two-sided Fisher's exact test was used to compare the occurrence of the thrombi in the wild-type and *+/hIC1* placentas. All analyses were performed using GraphPad Prism software. *$P < 0.05$, **$P < 0.01$, ***$P < 0.001$, ****$P < 0.0001$, n.s. = not significant.

Acknowledgments

Authors would like to express gratitude to Christopher Krapp, Lisa Vrooman, Joel Rurik, Olga Smirnova, Jonathan Schug, Klaus Kaestner, and Colin Conine for their guidance on this study. This work was supported by National Institutes of Health grant GM-051279-28 and R35HL140018-05, National Institute of Arthritis and Musculoskeletal and Skin Diseases grant 5T32AR053461.

Author Contributions

S.C. and M.S.B. designed the study. S.C. and J.L.T. performed experiments and maintained mouse lines. S.K.H. generated *⊿H19* allele. S.C., D.F., J.A.E. and L.L. evaluated cardiac histology. E.A.R. and X.C. evaluated placental histology. S.C. and Y.L. analyzed RNA-seq data. N.A.L. assisted in experiments for revision. S.C. and M.S.B. wrote the manuscript with input from all authors.

Competing Interests

The authors declare no competing interests.

Data Availability

RNA sequencing data are deposited in GEO database under the accession number GSE199377.

References

Abi Habib, W., Brioude, F., Azzi, S., Salem, J., Das Neves, C., Personnier, C., Chantot-Bastaraud, S.,

494 Keren, B., Le Bouc, Y., Harbison, M. D., & Netchine, I. (2017). 11p15 ICR1 Partial Deletions
495 Associated with IGF2/H19 DMR Hypomethylation and Silver–Russell Syndrome. *Human Mutation*.
496 https://doi.org/10.1002/humu.23131
497 Andrews, S., Krueger, F., Seconds-Pichon, A., Biggins, F., & Wingett, S. (2015). *FastQC. A quality*
498 *control tool for high throughput sequence data. Babraham Bioinformatics*. Babraham Institute.
499 Aykroyd, B. R. L., Tunster, S. J., & Sferruzzi-Perri, A. N. (2022). Loss of imprinting of the Igf2-H19
500 ICR1 enhances placental endocrine capacity via sex-specific alterations in signalling pathways in
501 the mouse . *Development*, *149*(1). https://doi.org/10.1242/dev.199811
502 Barak, Y., Hemberger, M., & Sucov, H. M. (2019). Phases and Mechanisms of Embryonic
503 Cardiomyocyte Proliferation and Ventricular Wall Morphogenesis. *Pediatric Cardiology*, *40*(7),
504 1359–1366. https://doi.org/10.1007/s00246-019-02164-6
505 Barlow, D. P., & Bartolomei, M. S. (2014). Genomic imprinting in mammals. *Cold Spring Harbor*
506 *Perspectives in Biology*. https://doi.org/10.1101/cshperspect.a018382
507 Begemann, M., Zirn, B., Santen, G., Wirthgen, E., Soellner, L., Büttel, H.-M., Schweizer, R., van
508 Workum, W., Binder, G., & Eggermann, T. (2015). Paternally Inherited IGF2 Mutation and Growth
509 Restriction . *New England Journal of Medicine*, *373*(4). https://doi.org/10.1056/nejmoa1415227
510 Borensztein, M., Viengchareun, S., Montarras, D., Journot, L., Binart, N., Lombès, M., & Dandolo, L.
511 (2012). Double Myod and Igf2 inactivation promotes brown adipose tissue development by
512 increasing Prdm16 expression. *FASEB Journal*. https://doi.org/10.1096/fj.12-208496
513 Chang, S., & Bartolomei, M. S. (2020). Modeling human epigenetic disorders in mice: Beckwith-
514 Wiedemann syndrome and Silver-Russell syndrome. In *DMM Disease Models and Mechanisms*
515 (Vol. 13, Issue 5). https://doi.org/10.1242/dmm.044123
516 Chen, C. P., Chang, S. Y., Lin, C. J., Chern, S. R., Wu, P. S., Chen, S. W., Lai, S. T., Chuang, T. Y.,
517 Chen, W. L., Yang, C. W., & Wang, W. (2018). Prenatal diagnosis of a familial 5p14.3-p14.1
518 deletion encompassing CDH18, CDH12, PMCHL1, PRDM9 and CDH10 in a fetus with congenital
519 heart disease on prenatal ultrasound. *Taiwanese Journal of Obstetrics and Gynecology*, *57*(5).

https://doi.org/10.1016/j.tjog.2018.08.023

Choong, O. K., Chen, C. Y., Zhang, J., Lin, J. H., Lin, P. J., Ruan, S. C., Kamp, T. J., & Hsieh, P. C. H. (2019). Hypoxia-induced H19/YB-1 cascade modulates cardiac remodeling after infarction. *Theranostics*, *9*(22). https://doi.org/10.7150/thno.35218

Conigliaro, A., Costa, V., Lo Dico, A., Saieva, L., Buccheri, S., Dieli, F., Manno, M., Raccosta, S., Mancone, C., Tripodi, M., De Leo, G., & Alessandro, R. (2015). CD90+ liver cancer cells modulate endothelial cell phenotype through the release of exosomes containing H19 lncRNA. *Molecular Cancer*, *14*(1), 1–11. https://doi.org/10.1186/s12943-015-0426-x

Constância, M., Hemberger, M., Hughes, J., Dean, W., Ferguson-Smith, A., Fundele, R., Stewart, F., Kelsey, G., Fowden, A., Sibley, C., & Reik, W. (2002). Placental-specific IGF-II is a major modulator of placental and fetal growth. *Nature*, *417*(6892), 945–948. https://doi.org/10.1038/nature00819

DeChiara, T. M., Robertson, E. J., & Efstratiadis, A. (1991). Parental imprinting of the mouse insulin-like growth factor II gene. *Cell*. https://doi.org/10.1016/0092-8674(91)90513-X

Dobin, A., Davis, C. A., Schlesinger, F., Drenkow, J., Zaleski, C., Jha, S., Batut, P., Chaisson, M., & Gingeras, T. R. (2013). STAR: Ultrafast universal RNA-seq aligner. *Bioinformatics*, *29*(1). https://doi.org/10.1093/bioinformatics/bts635

Dor, Y., Camenisch, T. D., Itin, A., Fishman, G. I., McDonald, J. A., Carmeliet, P., & Keshet, E. (2001). A novel role for VEGF in endocardial cushion formation and its potential contribution to congenital heart defects. *Development*, *128*(9). https://doi.org/10.1242/dev.128.9.1531

Drewell, R. A., Brenton, J. D., Ainscough, J. F. X., Barton, S. C., Hilton, K. J., Arney, K. L., Dandolo, L., & Surani, M. A. (2000). Deletion of a silencer element disrupts H19 imprinting independently of a DNA methylation epigenetic switch. *Development*.

Eggermann, T., Buiting, K., & Temple, I. K. (2011). Clinical utility gene card for: Silver-Russell syndrome. *European Journal of Human Genetics*. https://doi.org/10.1038/ejhg.2010.202

Eisenberg, L. M., & Markwald, R. R. (1995). Molecular regulation of atrioventricular valvuloseptal

546 morphogenesis. In *Circulation Research* (Vol. 77, Issue 1). https://doi.org/10.1161/01.RES.77.1.1

547 Engel, N., West, A. G., Felsenfeld, G., & Bartolomei, M. S. (2004). Antagonism between DNA

548 hypermethylation and enhancer-blocking activity at the H19 DMD is uncovered by CpG mutations.

549 *Nature Genetics*. https://doi.org/10.1038/ng1399

550 Esquiliano, D. R., Guo, W., Liang, L., Dikkes, P., & Lopez, M. F. (2009). Placental Glycogen Stores are

551 Increased in Mice with H19 Null Mutations but not in those with Insulin or IGF Type 1 Receptor

552 Mutations. *Placenta*, *30*(8). https://doi.org/10.1016/j.placenta.2009.05.004

553 Freschi, A., Del Prete, R., Pignata, L., Cecere, F., Manfrevola, F., Mattia, M., Cobellis, G., Sparago, A.,

554 Bartolomei, M. S., Riccio, A., & Cerrato, F. (2021). The number of the CTCF binding sites of the

555 H19/IGF2:IG-DMR correlates with DNA methylation and expression imprinting in a humanized

556 mouse model. *Human Molecular Genetics*, *30*(16). https://doi.org/10.1093/hmg/ddab132

557 Freschi, A., Hur, S. K., Valente, F. M., Ideraabdullah, F. Y., Sparago, A., Gentile, M. T., Oneglia, A., Di

558 Nucci, D., Colucci-D'Amato, L., Thorvaldsen, J. L., Bartolomei, M. S., Riccio, A., & Cerrato, F.

559 (2018). Tissue-specific and mosaic imprinting defects underlie opposite congenital growth disorders

560 in mice. *PLoS Genetics*. https://doi.org/10.1371/journal.pgen.1007243

561 Gabory, A., Jammes, H., & Dandolo, L. (2010). The H19 locus: Role of an imprinted non-coding RNA in

562 growth and development. In *BioEssays*. https://doi.org/10.1002/bies.200900170

563 Gabory, A., Ripoche, M. A., Le Digarcher, A., Watrin, F., Ziyyat, A., Forné, T., Jammes, H., Ainscough,

564 J. F. X., Surani, M. A., Journot, L., & Dandolo, L. (2009). H19 acts as a trans regulator of the

565 imprinted gene network controlling growth in mice. *Development*.

566 https://doi.org/10.1242/dev.036061

567 García-Padilla, C., Domínguez, J. N., Aránega, A. E., & Franco, D. (2019). Differential chamber-specific

568 expression and regulation of long non-coding RNAs during cardiac development. *Biochimica et*

569 *Biophysica Acta - Gene Regulatory Mechanisms*, *1862*(10), 194435.

570 https://doi.org/10.1016/j.bbagrm.2019.194435

571 Ghanim, M., Rossignol, S., Delobel, B., Irving, M., Miller, O., Devisme, L., Plennevaux, J. L.,

572 Lucidarme-Rossi, S., Manouvrier, S., Salah, A., Chivu, O., Netchine, I., & Vincent-Delorme, C.
573 (2013). Possible association between complex congenital heart defects and 11p15 hypomethylation
574 in three patients with severe Silver-Russell syndrome. *American Journal of Medical Genetics, Part*
575 *A*, *161*(3), 572–577. https://doi.org/10.1002/ajmg.a.35691
576 Gicquel, C., Rossignol, S., Cabrol, S., Houang, M., Steunou, V., Barbu, V., Danton, F., Thibaud, N., Le
577 Merrer, M., Burglen, L., Bertrand, A. M., Netchine, I., & Le Bouc, Y. (2005). Epimutation of the
578 telomeric imprinting center region on chromosome 11p15 in Silver-Russell syndrome. *Nature*
579 *Genetics*, *37*(9), 1003–1007. https://doi.org/10.1038/ng1629
580 Greco, S., Zaccagnini, G., Perfetti, A., Fuschi, P., Valaperta, R., Voellenkle, C., Castelvecchio, S.,
581 Gaetano, C., Finato, N., Beltrami, A. P., Menicanti, L., & Martelli, F. (2016). Long noncoding RNA
582 dysregulation in ischemic heart failure. *Journal of Translational Medicine*, *14*(1), 1–14.
583 https://doi.org/10.1186/s12967-016-0926-5
584 Haley, V. L., Barnes, D. J., Sandovici, I., Constancia, M., Graham, C. F., Pezzella, F., Bühnemann, C.,
585 Carter, E. J., & Hassan, A. B. (2012). Igf2 pathway dependency of the Trp53 developmental and
586 tumour phenotypes. *EMBO Molecular Medicine*. https://doi.org/10.1002/emmm.201101105
587 Han, L., Szabó, P. E., & Mann, J. R. (2010). Postnatal survival of mice with maternal duplication of distal
588 chromosome 7 induced by a Igf2/H19 imprinting control region lacking insulator function. *PLoS*
589 *Genetics*. https://doi.org/10.1371/journal.pgen.1000803
590 Harris, L. K., & Westwood, M. (2012). Biology and significance of signalling pathways activated by
591 IGF-II. *Growth Factors*, *30*(1), 1–12. https://doi.org/10.3109/08977194.2011.640325
592 Hobuß, L., Foinquinos, A., Jung, M., Kenneweg, F., Xiao, K., Wang, Y., Zimmer, K., Remke, J., Just, A.,
593 Nowak, J., Schmidt, A., Pich, A., Mazlan, S., Reamon-Buettner, S. M., Ramos, G. C., Frantz, S.,
594 Viereck, J., Loyer, X., Boulanger, C., … Thum, T. (2020). Pleiotropic cardiac functions controlled
595 by ischemia-induced lncRNA H19. *Journal of Molecular and Cellular Cardiology*, *146*(July 2019),
596 43–59. https://doi.org/10.1016/j.yjmcc.2020.07.001
597 Hubert, F., Payan, S. M., & Rochais, F. (2018). FGF10 Signaling in Heart Development, Homeostasis,

598 Disease and Repair. In *Frontiers in Genetics* (Vol. 9). https://doi.org/10.3389/fgene.2018.00599

599 Hur, S. K., Freschi, A., Ideraabdullah, F., Thorvaldsen, J. L., Luense, L. J., Weller, A. H., Berger, S. L.,

600 Cerrato, F., Riccio, A., & Bartolomei, M. S. (2016). Humanized H19/Igf2 locus reveals diverged

601 imprinting mechanism between mouse and human and reflects Silver-Russell syndrome phenotypes.

602 *Proceedings of the National Academy of Sciences of the United States of America*.

603 https://doi.org/10.1073/pnas.1603066113

604 Keniry, A., Oxley, D., Monnier, P., Kyba, M., Dandolo, L., Smits, G., & Reik, W. (2012). The H19

605 lincRNA is a developmental reservoir of miR-675 that suppresses growth and Igf1r. *Nature Cell*

606 *Biology*. https://doi.org/10.1038/ncb2521

607 Kochilas, L. K., Li, J., Jin, F., Buck, C. A., & Epstein, J. A. (1999). p57Kip2expression is enhanced

608 during mid-cardiac murine development and is restricted to trabecular myocardium. *Pediatric*

609 *Research*, *45*(5). https://doi.org/10.1203/00006450-199905010-00004

610 Kruithof, B. P. T., Krawitz, S. A., & Gaussin, V. (2007). Atrioventricular valve development during late

611 embryonic and postnatal stages involves condensation and extracellular matrix remodeling.

612 *Developmental Biology*, *302*(1). https://doi.org/10.1016/j.ydbio.2006.09.024

613 Lee, J. H., Gao, C., Peng, G., Greer, C., Ren, S., Wang, Y., & Xiao, X. (2011). Analysis of transcriptome

614 complexity through RNA sequencing in normal and failing murine hearts. *Circulation Research*,

615 *109*(12), 1332–1341. https://doi.org/10.1161/CIRCRESAHA.111.249433

616 Li, P., Cavallero, S., Gu, Y., Chen, T. H. P., Hughes, J., Hassan, A. B., Brüning, J. C., Pashmforoush, M.,

617 & Sucov, H. M. (2011). IGF signaling directs ventricular cardiomyocyte proliferation during

618 embryonic heart development. *Development*, *138*(9), 1795–1805.

619 https://doi.org/10.1242/dev.054338

620 Liao, J., Zeng, T. B., Pierce, N., Tran, D. A., Singh, P., Mann, J. R., & Szabó, P. E. (2021). Prenatal

621 correction of IGF2 to rescue the growth phenotypes in mouse models of Beckwith-Wiedemann and

622 Silver-Russell syndromes. *Cell Reports*, *34*(6). https://doi.org/10.1016/j.celrep.2021.108729

623 Lopez, M. F., Dikkes, P., Zurakowski, D., & Villa-Komaroff, L. (1996). Insulin-like growth factor II

affects the appearance and glycogen content of glycogen cells in the murine placenta. *Endocrinology*, *137*(5). https://doi.org/10.1210/endo.137.5.8612553

Love, M. I., Huber, W., & Anders, S. (2014). Moderated estimation of fold change and dispersion for RNA-seq data with DESeq2. *Genome Biology*, *15*(12). https://doi.org/10.1186/s13059-014-0550-8

Marsh, B., & Blelloch, R. (2020). Single nuclei RNA-seq of mouse placental labyrinth development. *ELife*, *9*. https://doi.org/10.7554/eLife.60266

Maslen, C. L. (2018). Recent advances in placenta-heart interactions. *Frontiers in Physiology*, *9*(JUN), 1–9. https://doi.org/10.3389/fphys.2018.00735

Matthiesen, N. B., Henriksen, T. B., Agergaard, P., Gaynor, J. W., Bach, C. C., Hjortdal, V. E., & Østergaard, J. R. (2016). Congenital Heart Defects and Indices of Placental and Fetal Growth in a Nationwide Study of 924 422 Liveborn Infants. *Circulation*, *134*(20), 1546–1556. https://doi.org/10.1161/CIRCULATIONAHA.116.021793

Mi, H., Muruganujan, A., Ebert, D., Huang, X., & Thomas, P. D. (2019). PANTHER version 14: More genomes, a new PANTHER GO-slim and improvements in enrichment analysis tools. *Nucleic Acids Research*, *47*(D1). https://doi.org/10.1093/nar/gky1038

Mootha, V. K., Lindgren, C. M., Eriksson, K. F., Subramanian, A., Sihag, S., Lehar, J., Puigserver, P., Carlsson, E., Ridderstråle, M., Laurila, E., Houstis, N., Daly, M. J., Patterson, N., Mesirov, J. P., Golub, T. R., Tamayo, P., Spiegelman, B., Lander, E. S., Hirschhorn, J. N., … Groop, L. C. (2003). PGC-1α-responsive genes involved in oxidative phosphorylation are coordinately downregulated in human diabetes. *Nature Genetics*, *34*(3). https://doi.org/10.1038/ng1180

Penny, D. J., & Vick, G. W. (2011). Ventricular septal defect. *The Lancet*, *377*(9771), 1103–1112. https://doi.org/10.1016/S0140-6736(10)61339-6

Perez-Garcia, V., Fineberg, E., Wilson, R., Murray, A., Mazzeo, C. I., Tudor, C., Sienerth, A., White, J. K., Tuck, E., Ryder, E. J., Gleeson, D., Siragher, E., Wardle-Jones, H., Staudt, N., Wali, N., Collins, J., Geyer, S., Busch-Nentwich, E. M., Galli, A., … Hemberger, M. (2018). Placentation defects are highly prevalent in embryonic lethal mouse mutants. *Nature*, *555*(7697), 463–468.

https://doi.org/10.1038/nature26002

Poirier, F., Chan, C. T. J., Timmons, P. M., Robertson, E. J., Evans, M. J., & Rigby, P. W. J. (1991). The murine H19 gene is activated during embryonic stem cell differentiation in vitro and at the time of implantation in the developing embryo. *Development*, *113*(4). https://doi.org/10.1242/dev.113.4.1105

Rochais, F., Sturny, R., Chao, C. M., Mesbah, K., Bennett, M., Mohun, T. J., Bellusci, S., & Kelly, R. G. (2014). FGF10 promotes regional foetal cardiomyocyte proliferation and adult cardiomyocyte cell-cycle re-entry. *Cardiovascular Research*, *104*(3). https://doi.org/10.1093/cvr/cvu232

Rychik, J., Goff, D., McKay, E., Mott, A., Tian, Z., Licht, D. J., & Gaynor, J. W. (2018). Characterization of the Placenta in the Newborn with Congenital Heart Disease: Distinctions Based on Type of Cardiac Malformation. *Pediatric Cardiology*, *39*(6), 1165–1171. https://doi.org/10.1007/s00246-018-1876-x

Sandovici, I., Georgopoulou, A., Pérez-García, V., Hufnagel, A., López-Tello, J., Lam, B. Y. H., Schiefer, S. N., Gaudreau, C., Santos, F., Hoelle, K., Yeo, G. S. H., Burling, K., Reiterer, M., Fowden, A. L., Burton, G. J., Branco, C. M., Sferruzzi-Perri, A. N., & Constância, M. (2022). The imprinted Igf2-Igf2r axis is critical for matching placental microvasculature expansion to fetal growth. *Developmental Cell*, *57*(1), 63-79.e8. https://doi.org/10.1016/j.devcel.2021.12.005

SanMiguel, J. M., Abramowitz, L. K., & Bartolomei, M. S. (2018). Imprinted gene dysregulation in a Tet1 null mouse model is stochastic and variable in the germline and offspring. *Development (Cambridge)*, *145*(7). https://doi.org/10.1242/dev.160622

Savolainen, S. M., Foley, J. F., & Elmore, S. A. (2009). Histology atlas of the developing mouse heart with emphasis on E11.5 to E18.5. *Toxicologic Pathology*, *37*(4), 395–414. https://doi.org/10.1177/0192623309335060

Schindelin, J., Arganda-Carreras, I., Frise, E., Kaynig, V., Longair, M., Pietzsch, T., Preibisch, S., Rueden, C., Saalfeld, S., Schmid, B., Tinevez, J. Y., White, D. J., Hartenstein, V., Eliceiri, K., Tomancak, P., & Cardona, A. (2012). Fiji: An open-source platform for biological-image analysis.

In *Nature Methods* (Vol. 9, Issue 7). https://doi.org/10.1038/nmeth.2019

Serra, A., Eirich, K., Winkler, A. K., Mrasek, K., Ghring, G., Barbi, G., Cario, H., Schlegelberger, B., Pokora, B., Liehr, T., Leriche, C., Henne-Bruns, D., Barth, T. F., & Schindler, D. (2012). Shared copy number variation in simultaneous nephroblastoma and neuroblastoma due to Fanconi anemia. *Molecular Syndromology*, *3*(3), 120–130. https://doi.org/10.1159/000341935

Shen, H., Cavallero, S., Estrada, K. D., Sandovici, I., Kumar, S. R., Makita, T., Lien, C. L., Constancia, M., & Sucov, H. M. (2015). Extracardiac control of embryonic cardiomyocyte proliferation and ventricular wall expansion. *Cardiovascular Research*, *105*(3), 271–278. https://doi.org/10.1093/cvr/cvu269

Shen, H., Gan, P., Wang, K., Darehzereshki, A., Wang, K., Ram Kumar, S., Lien, C. L., Patterson, M., Tao, G., & Sucov, H. M. (2020). Mononuclear diploid cardiomyocytes support neonatal mouse heart regeneration in response to paracrine IGF2 signaling. *ELife*, *9*, 1–24. https://doi.org/10.7554/eLife.53071

Sibley, C. P., Coan, P. M., Dean, W., Hughes, J., Smith, P., Reik, W., & Burton, G. J. (2004). *Regulates the Diffusional Exchange Characteristics of the Mouse Placenta*. *2*.

Snider, P., & Conway, S. J. (2011). Probing human cardiovascular congenital disease using transgenic mouse models. In *Progress in Molecular Biology and Translational Science* (1st ed., Vol. 100). Elsevier Inc. https://doi.org/10.1016/B978-0-12-384878-9.00003-0

Soellner, L., Kraft, F., Sauer, S., Begemann, M., Kurth, I., Elbracht, M., & Eggermann, T. (2019). Search for cis-acting factors and maternal effect variants in Silver-Russell patients with ICR1 hypomethylation and their mothers. *European Journal of Human Genetics*, *27*(1). https://doi.org/10.1038/s41431-018-0269-1

Soemedi, R., Wilson, I. J., Bentham, J., Darlay, R., Töpf, A., Zelenika, D., Cosgrove, C., Setchfield, K., Thornborough, C., Granados-Riveron, J., Blue, G. M., Breckpot, J., Hellens, S., Zwolinkski, S., Glen, E., Mamasoula, C., Rahman, T. J., Hall, D., Rauch, A., … Keavney, B. D. (2012). Contribution of global rare copy-number variants to the risk of sporadic congenital heart disease.

American Journal of Human Genetics, *91*(3). https://doi.org/10.1016/j.ajhg.2012.08.003

Spicer, D. E., Hsu, H. H., Co-Vu, J., Anderson, R. H., & Fricker, F. J. (2014). Ventricular septal defect. *Orphanet Journal of Rare Diseases*, *9*, 144. https://doi.org/10.1186/s13023-014-0144-2

Subramanian, A., Tamayo, P., Mootha, V. K., Mukherjee, S., Ebert, B. L., Gillette, M. A., Paulovich, A., Pomeroy, S. L., Golub, T. R., Lander, E. S., & Mesirov, J. P. (2005). Gene set enrichment analysis: A knowledge-based approach for interpreting genome-wide expression profiles. *Proceedings of the National Academy of Sciences of the United States of America*, *102*(43). https://doi.org/10.1073/pnas.0506580102

Sullivan, K. E., & Black, L. D. (2013). The role of cardiac fibroblasts in extracellular matrix-mediated signaling during normal and pathological cardiac development. *Journal of Biomechanical Engineering*, *135*(7). https://doi.org/10.1115/1.4024349

Thorvaldsen, J. L., Duran, K. L., & Bartolomei, M. S. (1998). Deletion of the H19 differentially methylated domain results in loss of imprinted expression of H19 and Igf2. *Genes and Development*. https://doi.org/10.1101/gad.12.23.3693

Thorvaldsen, J. L., Fedoriw, A. M., Nguyen, S., & Bartolomei, M. S. (2006). Developmental Profile of H19 Differentially Methylated Domain (DMD) Deletion Alleles Reveals Multiple Roles of the DMD in Regulating Allelic Expression and DNA Methylation at the Imprinted H19/Igf2 Locus. *Molecular and Cellular Biology*. https://doi.org/10.1128/mcb.26.4.1245-1258.2006

Thorvaldsen, J. L., Mann, M. R. W., Nwoko, O., Duran, K. L., & Bartolomei, M. S. (2002). Analysis of Sequence Upstream of the Endogenous H19 Gene Reveals Elements Both Essential and Dispensable for Imprinting. *Molecular and Cellular Biology*. https://doi.org/10.1128/mcb.22.8.2450-2462.2002

Ueno, M., Lee, L. K., Chhabra, A., Kim, Y. J., Sasidharan, R., VanHandel, B., Wang, Y., Kamata, M., Kamran, P., Sereti, K. I., Ardehali, R., Jiang, M., & Mikkola, H. K. A. (2013). C-Met-Dependent Multipotent Labyrinth Trophoblast Progenitors Establish Placental Exchange Interface. *Developmental Cell*, *27*(4), 373–386. https://doi.org/10.1016/j.devcel.2013.10.019

Vega-Hernández, M., Kovacs, A., de Langhe, S., & Ornitz, D. M. (2011). FGF10/FGFR2b signaling is

728 essential for cardiac fibroblast development and growth of the myocardium. *Development*, *138*(15).
729 https://doi.org/10.1242/dev.064410
730 Von Gise, A., & Pu, W. T. (2012). Endocardial and epicardial epithelial to mesenchymal transitions in
731 heart development and disease. *Circulation Research*, *110*(12), 1628–1645.
732 https://doi.org/10.1161/CIRCRESAHA.111.259960
733 Vrooman, L. A., Rhon-Calderon, E. A., Chao, O. Y., Nguyen, D. K., Narapareddy, L., Dahiya, A. K.,
734 Putt, M. E., Schultz, R. M., & Bartolomei, M. S. (2020). Assisted reproductive technologies induce
735 temporally specific placental defects and the preeclampsia risk marker sFLT1 in mouse.
736 *Development (Cambridge, England)*, *147*(11). https://doi.org/10.1242/dev.186551
737 Wakeling, E. L., Brioude, F., Lokulo-Sodipe, O., O'Connell, S. M., Salem, J., Bliek, J., Canton, A. P. M.,
738 Chrzanowska, K. H., Davies, J. H., Dias, R. P., Dubern, B., Elbracht, M., Giabicani, E., Grimberg,
739 A., Grønskov, K., Hokken-Koelega, A. C. S., Jorge, A. A., Kagami, M., Linglart, A., … Netchine, I.
740 (2017). Diagnosis and management of Silver-Russell syndrome: First international consensus
741 statement. *Nature Reviews Endocrinology*, *13*(2), 105–124. https://doi.org/10.1038/nrendo.2016.138
742 Wang, Y., Sun, X., & Sun, X. (2021). The Functions of LncRNA H19 in the Heart. In *Heart Lung and*
743 *Circulation*. https://doi.org/10.1016/j.hlc.2021.10.022
744 Woods, L., Perez-Garcia, V., & Hemberger, M. (2018). Regulation of Placental Development and Its
745 Impact on Fetal Growth—New Insights From Mouse Models. *Frontiers in Endocrinology*,
746 *9*(September), 1–18. https://doi.org/10.3389/fendo.2018.00570
747 Yang, H., Wang, H., & Jaenisch, R. (2014). Generating genetically modified mice using CRISPR/Cas-
748 mediated genome engineering. *Nature Protocols*, *9*(8). https://doi.org/10.1038/nprot.2014.134
749

Supplemental Information

Generation of *⊿H19* allele. Two pairs of gRNA targeting the *H19* gene are listed in Supplemental Table 1. gRNA was prepared following a protocol from Yang et al. (Yang et al., 2014) with modifications. px335 plasmid (Addgene, Watertown, MA) was PCR amplified using Phusion high-fidelity DNA polymerase (New England Biolabs, Ipswich, MA) and the primer set listed in Supplemental Table 1. ~117bp PCR product was gel-purified using the Gel Extraction kit (Qiagen, Hilden, Germany) according to the manufacturer's instruction. Using the gel-purified product as template, *in vitro* transcription of gRNA was setup using T7 High Yield RNA Synthesis kit (New England Biolabs) according to manufacturer's instructions. Transcribed gRNA was purified using the MEGAclear kit (Life Technologies, Carlsbad, CA) according to manufacturer's instructions. 50 ng/µl left and right sgRNA together with 100 ng/µl Cas9 mRNA was injected per zygote stage embryo by the Transgenic and Chimeric Mouse Facility at the University of Pennsylvania. The targeted allele was validated using Southern blot as previously described (Thorvaldsen et al., 1998) and PCR and sequencing across junctions of *⊿H19* alleles. Obtained chimeras and germ line transmission animals were PCR-genotyped for the *⊿H19* allele using primers (Supplemental Table 1).

Genotyping. Mouse genomic DNA for PCR genotyping was isolated from each animal as previously described (SanMiguel et al., 2018). Primers used for sex genotyping and genotyping of *hIC1, ⊿H19* and *⊿3.8* alleles are listed in Supplemental Table 1. For all genotypes, the maternal allele is listed first and the paternal allele second.

RNA Sequencing library preparation and analysis. E12.5 hearts were lysed with Collagenase (Sigma-Aldrich), Dispase II (Sigma-Aldrich), and DNase I (Sigma-Aldrich). Cardiac endothelial cells were collected using MACS CD31 microbeads (Miltenyi Biotec, Bergisch Gladbach, Germany) and RNA was isolated using RNeasy Micro kit (Qiagen). After confirming RNA integrity using Bioanalyzer (Agilent Technologies, Santa Clara, CA), mRNA library was generated from 25ng RNA using NEBNext Poly(A) mRNA Magnetic Isolation Module and Ultra II RNA Library Prep Kit (New England Biolabs). Library quality was assessed by Bioanalyzer (Agilent Technologies) and TapeStation (Agilent Technologies). Sequencing was performed on NovaSeq 6000 (Illumina, San Diego, CA). Quality of raw fastq reads was assessed using FastQC version 0.11.5 (Andrews et al., 2015). Reads were aligned to the GRCm38/mm10 reference using STAR version 2.4.0i with default parameters and maximum fragment size of 2000 bp (Dobin et al., 2013). Properly paired primary alignments were retained for downstream analysis using Samtools version 1.9. Count matrices were generated using FeatureCounts version 1.6.2 against RefSeq gene annotation and read into DESeq2 (Love et al., 2014) to perform normalization and statistical analysis.

Supplemental Figure 1. Supplementary data for anomalies observed in +/*hIC1* placentas.
(A) Quantification of ventricular wall thickness (µm), measured from E15.5 wild-type and *+/hIC1* hearts (mean ± SD). 4 wild-type and 3 *+/hIC1* embryos from two different litters were examined. (B) Fetal to placental weight ratios of the wild-type (blue) and *+/hIC1* (red) samples at E11.5, E12.5, E14.5 and E15.5. Each data point represents an average ratio of each genotype from one litter. (C) Junctional zone (Jz) to labyrinth (Lb) ratio in E17.5 wild-type and *+/hIC1* placentas. (D) Example of labyrinth zones that were used to quantify the microvessel density in CD34 immunostained E17.5 wild-type and *+/hIC1* placental sections from Figure 3G. Thrombi in *+/hIC1* placentas were excluded. (E) (Left) Representative images of PAS staining counterstained with hematoxylin on E17.5 wild-type and *+/hIC1* male placental sections. (Right) Quantification of PAS stained images. (F) Relative total expression of miR-675-3p and miR-675-5p in E15.5 wild-type and *+/hIC1* placentas (mean ± SD). (A, C, E, F) Each data point represents an individual conceptus from different litters. Scale bars = 1mm. Statistics used are (A, C, E, F) multiple unpaired t-tests, (B) multiple paired t-test. *$P < 0.05$, **$P < 0.01$, ***$P < 0.001$, ****$P < 0.0001$, ns = not significant.

Supplemental Figure 2. Serial cross-sections of E15.5 *+/hIC1* embryonic heart with BPV.

Sequential histological sections demonstrating the bicuspid pulmonary valve (BPV) phenotype. Rudimentary anterior cusp can be seen fused with the right pulmonary cusp (raphe) in sections denoted by * above the pulmonary valve.

Supplemental Figure 3. Characterization of *⊿H19* allele.

(A) Targeting strategy to generate the *⊿H19* allele. The endogenous *H19* locus is shown with restriction sites, gRNA locations used to generate the deletion and binding sites for probes used in Southern blot analysis (thick lines). (B) Southern blot analysis of *⊿H19* allele. Founder 4131 line was generated using gRNA pair A, and founder 4133 line was generated using gRNA pair B (Supplemental Table 1). 3' probe and 5' probe were hybridized to XbaI- and KpnI-digested DNA, respectively. The sizes of the DNA fragments are shown on the right. (C) Allele-specific *Igf2* expression in wild-type and *⊿H19/+* neonatal tongue, heart and liver analyzed by restriction fragment length polymorphism (RFLP). Ladder, genotypes and c (*Mus castaneus*, paternal) and b (C57BL/6, maternal) allele controls are indicated above each gel. Quantification of band densitometry is shown below each gel, with percent of maternal allele expression relative to paternal allele indicated. No expression from the maternal *Igf2* allele was observed in liver. (D) Embryonic and neonatal body weight of the wild-type (blue) and *⊿H19/+* (green) samples at E11.5, E12.5, E14.5, E17.5, E18.5 and PN0 (mean ± SD). 6 litters for E11.5, 6 litters for E12.5, 3 litters for E14.5, 11 litters for E17.5, 3 litters for E18.5,14 litters for PN0 are presented. (E) Body weight of +/*⊿H19* neonates (mean ± SD). 3 litters are presented. (D, E) Each data point represents an average weight of each genotype from one litter. Paired Student's t-test; **P* < 0.05, ***P* < 0.01, ****P* < 0.001, *****P* < 0.0001, ns = not significant.

Supplemental Figure 4. Supplementary data for rescue upon maternal *⊿H19* transmission.

(A) Ratio of wild-type, *⊿H19/+, +/hIC1* and *⊿H19/hIC1* embryos observed in E11.5 and E17.5 litters (>5 pups) (mean ± SD). Each data point represents one litter. (B) (Left) Relative placental weights of E17.5 wild-type, *⊿H19/+, +/hIC1* and *⊿H19/hIC1* samples, normalized to the average placental weight of the wild-type littermates (mean ± SD). (Right) Fetal to placental weight ratio in E17.5 wild-type, *⊿H19/+, +/hIC1* and *⊿H19/hIC1* samples (mean ± SD). (C) Relative total expression of *H19* and *Igf2* in E17.5 wild-type, *⊿H19/+, +/hIC1* and *⊿H19/hIC1* liver and tongue samples (mean ± SD). (D) %Area of thrombotic clots in *⊿H19/hIC1* placentas, relative to labyrinth zone. (B, C) Each data point represents an individual conceptus from different litters. Statistics used are (A) Paired Student's t-test, (B, C) One-way ANOVA with Tukey's multiple comparisons test; **P* < 0.05, ***P* < 0.01, ****P* < 0.001, *****P* < 0.0001, ns = not significant.

Supplemental Figure 5. Supplementary data for rescue upon maternal *⊿3.8* transmission.

(A) (Left) Relative placental weights of E17.5 wild-type, *⊿3.8/+, +/hIC1* and *⊿3.8/hIC1* samples, normalized to the average placental weight of the wild-type littermates (mean ± SD). (Right) Fetal to placental weight ratio in E17.5 wild-type, *⊿3.8/+, +/hIC1* and *⊿3.8/hIC1* samples (mean ± SD). (B) Relative total expression of *H19* and *Igf2* in E17.5 wild-type, *⊿3.8/+, +/hIC1* and *⊿3.8/hIC1* liver and tongue samples (mean ± SD). (C) Junctional zone (Jz) to labyrinth (Lb) ratio in E17.5 wild-type, *⊿3.8/+, +/hIC1* and *⊿3.8/hIC1* placentas. (A, B, C) Each data point represents an individual conceptus from different litters. One-way ANOVA with Tukey's multiple comparisons test; **P* < 0.05, ***P* < 0.01, ****P* < 0.001, *****P* < 0.0001, ns = not significant.

Supplemental Figure 6. Supplementary data for differential gene expression of *+/hIC1* hearts. (A) DAPI (blue) on E17.5 wild-type and *+/hIC1* hearts from Figure 6C. Images on the right are enlarged from the boxed area of images on the left. Scale bars = 100 µm. (B) Immunofluorescence staining for MF20 (red), collagen I (green), and DAPI (blue) on E17.5 *+/hIC1* hearts. Images on the right are enlarged from the boxed area of images on the left. Scale Bars = 100 µm. (C) Same-sex comparisons between *+/hIC1* and the wild-type samples analyzed by RNA sequencing. (D) Chromosomal distribution of DEGs from comparisons between *+/hIC1* and wild-type males and females.

Supplemental Figure 7. (A) Volcano plot depicting comparison of *⊿H19/hIC1* and wild-type cardiac endothelial cells. (B) Volcano plot depicting comparison of *+/hIC1* and *⊿H19/hIC1* cardiac endothelial cells. (C) GO pathways that are enriched for 46 DEGs between *+/hIC1* and *⊿H19/hIC1* samples.

Supplemental Figure 8. Enrichment tests for BRIDEAU_IMPRINTED_GENES using GSEA. Normalized enrichment score (NES), nominal p-value, enrichment plot and expression heatmap of the analyzed gene set comparing (A) *+/hIC1* and wild-type, (B) *⊿H19/+* and wild-type, (C) *⊿H19/hIC1* and wild-type cardiac endothelial cells.

Supplemental Figure 9. (A) Volcano plot depicting comparison of *+/hIC1* and *⊿3.8/hIC1* cardiac endothelial cells. (B) GO pathways that are enriched for 116 DEGs that are commonly differentially expressed in *+/hIC1* compared to wild-type and *⊿3.8/hIC1* samples. (C) Volcano plot depicting comparison of *⊿3.8/+* and wild-type cardiac endothelial cells.

Supplemental Figure 10. Enrichment tests for HALLMARK_HYPOXIA, GROSS_HYPOXIA_VIA_HIF1A_DN using GSEA.
Normalized enrichment score (NES), nominal p-value, enrichment plot and expression heatmap of the (A) HALLMARK_HYPOXIA, (B) GROSS_HYPOXIA_VIA_HIF1A_DN gene set comparing *+/hIC1* and wild-type cardiac endothelial cells.

872

873 **Supplemental References**

874 Abi Habib, W., Brioude, F., Azzi, S., Salem, J., Das Neves, C., Personnier, C., Chantot-Bastaraud, S.,
875 Keren, B., Le Bouc, Y., Harbison, M. D., & Netchine, I. (2017). 11p15 ICR1 Partial Deletions
876 Associated with IGF2/H19 DMR Hypomethylation and Silver–Russell Syndrome. *Human Mutation*.
877 https://doi.org/10.1002/humu.23131

878 Andrews, S., Krueger, F., Seconds-Pichon, A., Biggins, F., & Wingett, S. (2015). *FastQC. A quality*
879 *control tool for high throughput sequence data. Babraham Bioinformatics*. Babraham Institute.

880 Aykroyd, B. R. L., Tunster, S. J., & Sferruzzi-Perri, A. N. (2022). Loss of imprinting of the Igf2-H19
881 ICR1 enhances placental endocrine capacity via sex-specific alterations in signalling pathways in
882 the mouse . *Development*, *149*(1). https://doi.org/10.1242/dev.199811

883 Barak, Y., Hemberger, M., & Sucov, H. M. (2019). Phases and Mechanisms of Embryonic
884 Cardiomyocyte Proliferation and Ventricular Wall Morphogenesis. *Pediatric Cardiology*, *40*(7),
885 1359–1366. https://doi.org/10.1007/s00246-019-02164-6

886 Barlow, D. P., & Bartolomei, M. S. (2014). Genomic imprinting in mammals. *Cold Spring Harbor*
887 *Perspectives in Biology*. https://doi.org/10.1101/cshperspect.a018382

888 Begemann, M., Zirn, B., Santen, G., Wirthgen, E., Soellner, L., Büttel, H.-M., Schweizer, R., van
889 Workum, W., Binder, G., & Eggermann, T. (2015). Paternally Inherited IGF2 Mutation and Growth
890 Restriction . *New England Journal of Medicine*, *373*(4). https://doi.org/10.1056/nejmoa1415227

891 Borensztein, M., Viengchareun, S., Montarras, D., Journot, L., Binart, N., Lombès, M., & Dandolo, L.
892 (2012). Double Myod and Igf2 inactivation promotes brown adipose tissue development by
893 increasing Prdm16 expression. *FASEB Journal*. https://doi.org/10.1096/fj.12-208496

894 Chang, S., & Bartolomei, M. S. (2020). Modeling human epigenetic disorders in mice: Beckwith-
895 Wiedemann syndrome and Silver-Russell syndrome. In *DMM Disease Models and Mechanisms*
896 (Vol. 13, Issue 5). https://doi.org/10.1242/dmm.044123

897 Chen, C. P., Chang, S. Y., Lin, C. J., Chern, S. R., Wu, P. S., Chen, S. W., Lai, S. T., Chuang, T. Y.,

898 Chen, W. L., Yang, C. W., & Wang, W. (2018). Prenatal diagnosis of a familial 5p14.3-p14.1
899 deletion encompassing CDH18, CDH12, PMCHL1, PRDM9 and CDH10 in a fetus with congenital
900 heart disease on prenatal ultrasound. *Taiwanese Journal of Obstetrics and Gynecology*, *57*(5).
901 https://doi.org/10.1016/j.tjog.2018.08.023
902 Choong, O. K., Chen, C. Y., Zhang, J., Lin, J. H., Lin, P. J., Ruan, S. C., Kamp, T. J., & Hsieh, P. C. H.
903 (2019). Hypoxia-induced H19/YB-1 cascade modulates cardiac remodeling after infarction.
904 *Theranostics*, *9*(22). https://doi.org/10.7150/thno.35218
905 Conigliaro, A., Costa, V., Lo Dico, A., Saieva, L., Buccheri, S., Dieli, F., Manno, M., Raccosta, S.,
906 Mancone, C., Tripodi, M., De Leo, G., & Alessandro, R. (2015). CD90+ liver cancer cells modulate
907 endothelial cell phenotype through the release of exosomes containing H19 lncRNA. *Molecular*
908 *Cancer*, *14*(1), 1–11. https://doi.org/10.1186/s12943-015-0426-x
909 Constância, M., Hemberger, M., Hughes, J., Dean, W., Ferguson-Smith, A., Fundele, R., Stewart, F.,
910 Kelsey, G., Fowden, A., Sibley, C., & Reik, W. (2002). Placental-specific IGF-II is a major
911 modulator of placental and fetal growth. *Nature*, *417*(6892), 945–948.
912 https://doi.org/10.1038/nature00819
913 DeChiara, T. M., Robertson, E. J., & Efstratiadis, A. (1991). Parental imprinting of the mouse insulin-like
914 growth factor II gene. *Cell*. https://doi.org/10.1016/0092-8674(91)90513-X
915 Dobin, A., Davis, C. A., Schlesinger, F., Drenkow, J., Zaleski, C., Jha, S., Batut, P., Chaisson, M., &
916 Gingeras, T. R. (2013). STAR: Ultrafast universal RNA-seq aligner. *Bioinformatics*, *29*(1).
917 https://doi.org/10.1093/bioinformatics/bts635
918 Dor, Y., Camenisch, T. D., Itin, A., Fishman, G. I., McDonald, J. A., Carmeliet, P., & Keshet, E. (2001).
919 A novel role for VEGF in endocardial cushion formation and its potential contribution to congenital
920 heart defects. *Development*, *128*(9). https://doi.org/10.1242/dev.128.9.1531
921 Drewell, R. A., Brenton, J. D., Ainscough, J. F. X., Barton, S. C., Hilton, K. J., Arney, K. L., Dandolo, L.,
922 & Surani, M. A. (2000). Deletion of a silencer element disrupts H19 imprinting independently of a
923 DNA methylation epigenetic switch. *Development*.

924 Eggermann, T., Buiting, K., & Temple, I. K. (2011). Clinical utility gene card for: Silver-Russell
925 syndrome. *European Journal of Human Genetics*. https://doi.org/10.1038/ejhg.2010.202
926 Eisenberg, L. M., & Markwald, R. R. (1995). Molecular regulation of atrioventricular valvuloseptal
927 morphogenesis. In *Circulation Research* (Vol. 77, Issue 1). https://doi.org/10.1161/01.RES.77.1.1
928 Engel, N., West, A. G., Felsenfeld, G., & Bartolomei, M. S. (2004). Antagonism between DNA
929 hypermethylation and enhancer-blocking activity at the H19 DMD is uncovered by CpG mutations.
930 *Nature Genetics*. https://doi.org/10.1038/ng1399
931 Esquiliano, D. R., Guo, W., Liang, L., Dikkes, P., & Lopez, M. F. (2009). Placental Glycogen Stores are
932 Increased in Mice with H19 Null Mutations but not in those with Insulin or IGF Type 1 Receptor
933 Mutations. *Placenta*, *30*(8). https://doi.org/10.1016/j.placenta.2009.05.004
934 Freschi, A., Del Prete, R., Pignata, L., Cecere, F., Manfrevola, F., Mattia, M., Cobellis, G., Sparago, A.,
935 Bartolomei, M. S., Riccio, A., & Cerrato, F. (2021). The number of the CTCF binding sites of the
936 H19/IGF2:IG-DMR correlates with DNA methylation and expression imprinting in a humanized
937 mouse model. *Human Molecular Genetics*, *30*(16). https://doi.org/10.1093/hmg/ddab132
938 Freschi, A., Hur, S. K., Valente, F. M., Ideraabdullah, F. Y., Sparago, A., Gentile, M. T., Oneglia, A., Di
939 Nucci, D., Colucci-D'Amato, L., Thorvaldsen, J. L., Bartolomei, M. S., Riccio, A., & Cerrato, F.
940 (2018). Tissue-specific and mosaic imprinting defects underlie opposite congenital growth disorders
941 in mice. *PLoS Genetics*. https://doi.org/10.1371/journal.pgen.1007243
942 Gabory, A., Jammes, H., & Dandolo, L. (2010). The H19 locus: Role of an imprinted non-coding RNA in
943 growth and development. In *BioEssays*. https://doi.org/10.1002/bies.200900170
944 Gabory, A., Ripoche, M. A., Le Digarcher, A., Watrin, F., Ziyyat, A., Forné, T., Jammes, H., Ainscough,
945 J. F. X., Surani, M. A., Journot, L., & Dandolo, L. (2009). H19 acts as a trans regulator of the
946 imprinted gene network controlling growth in mice. *Development*.
947 https://doi.org/10.1242/dev.036061
948 García-Padilla, C., Domínguez, J. N., Aránega, A. E., & Franco, D. (2019). Differential chamber-specific
949 expression and regulation of long non-coding RNAs during cardiac development. *Biochimica et*

Biophysica Acta - Gene Regulatory Mechanisms, *1862*(10), 194435. https://doi.org/10.1016/j.bbagrm.2019.194435

Ghanim, M., Rossignol, S., Delobel, B., Irving, M., Miller, O., Devisme, L., Plennevaux, J. L., Lucidarme-Rossi, S., Manouvrier, S., Salah, A., Chivu, O., Netchine, I., & Vincent-Delorme, C. (2013). Possible association between complex congenital heart defects and 11p15 hypomethylation in three patients with severe Silver-Russell syndrome. *American Journal of Medical Genetics, Part A*, *161*(3), 572–577. https://doi.org/10.1002/ajmg.a.35691

Gicquel, C., Rossignol, S., Cabrol, S., Houang, M., Steunou, V., Barbu, V., Danton, F., Thibaud, N., Le Merrer, M., Burglen, L., Bertrand, A. M., Netchine, I., & Le Bouc, Y. (2005). Epimutation of the telomeric imprinting center region on chromosome 11p15 in Silver-Russell syndrome. *Nature Genetics*, *37*(9), 1003–1007. https://doi.org/10.1038/ng1629

Greco, S., Zaccagnini, G., Perfetti, A., Fuschi, P., Valaperta, R., Voellenkle, C., Castelvecchio, S., Gaetano, C., Finato, N., Beltrami, A. P., Menicanti, L., & Martelli, F. (2016). Long noncoding RNA dysregulation in ischemic heart failure. *Journal of Translational Medicine*, *14*(1), 1–14. https://doi.org/10.1186/s12967-016-0926-5

Haley, V. L., Barnes, D. J., Sandovici, I., Constancia, M., Graham, C. F., Pezzella, F., Bühnemann, C., Carter, E. J., & Hassan, A. B. (2012). Igf2 pathway dependency of the Trp53 developmental and tumour phenotypes. *EMBO Molecular Medicine*. https://doi.org/10.1002/emmm.201101105

Han, L., Szabó, P. E., & Mann, J. R. (2010). Postnatal survival of mice with maternal duplication of distal chromosome 7 induced by a Igf2/H19 imprinting control region lacking insulator function. *PLoS Genetics*. https://doi.org/10.1371/journal.pgen.1000803

Harris, L. K., & Westwood, M. (2012). Biology and significance of signalling pathways activated by IGF-II. *Growth Factors*, *30*(1), 1–12. https://doi.org/10.3109/08977194.2011.640325

Hobuß, L., Foinquinos, A., Jung, M., Kenneweg, F., Xiao, K., Wang, Y., Zimmer, K., Remke, J., Just, A., Nowak, J., Schmidt, A., Pich, A., Mazlan, S., Reamon-Buettner, S. M., Ramos, G. C., Frantz, S., Viereck, J., Loyer, X., Boulanger, C., … Thum, T. (2020). Pleiotropic cardiac functions controlled

by ischemia-induced lncRNA H19. *Journal of Molecular and Cellular Cardiology*, *146*(July 2019), 43–59. https://doi.org/10.1016/j.yjmcc.2020.07.001

Hubert, F., Payan, S. M., & Rochais, F. (2018). FGF10 Signaling in Heart Development, Homeostasis, Disease and Repair. In *Frontiers in Genetics* (Vol. 9). https://doi.org/10.3389/fgene.2018.00599

Hur, S. K., Freschi, A., Ideraabdullah, F., Thorvaldsen, J. L., Luense, L. J., Weller, A. H., Berger, S. L., Cerrato, F., Riccio, A., & Bartolomei, M. S. (2016). Humanized H19/Igf2 locus reveals diverged imprinting mechanism between mouse and human and reflects Silver-Russell syndrome phenotypes. *Proceedings of the National Academy of Sciences of the United States of America*. https://doi.org/10.1073/pnas.1603066113

Keniry, A., Oxley, D., Monnier, P., Kyba, M., Dandolo, L., Smits, G., & Reik, W. (2012). The H19 lincRNA is a developmental reservoir of miR-675 that suppresses growth and Igf1r. *Nature Cell Biology*. https://doi.org/10.1038/ncb2521

Kochilas, L. K., Li, J., Jin, F., Buck, C. A., & Epstein, J. A. (1999). p57Kip2expression is enhanced during mid-cardiac murine development and is restricted to trabecular myocardium. *Pediatric Research*, *45*(5). https://doi.org/10.1203/00006450-199905010-00004

Kruithof, B. P. T., Krawitz, S. A., & Gaussin, V. (2007). Atrioventricular valve development during late embryonic and postnatal stages involves condensation and extracellular matrix remodeling. *Developmental Biology*, *302*(1). https://doi.org/10.1016/j.ydbio.2006.09.024

Lee, J. H., Gao, C., Peng, G., Greer, C., Ren, S., Wang, Y., & Xiao, X. (2011). Analysis of transcriptome complexity through RNA sequencing in normal and failing murine hearts. *Circulation Research*, *109*(12), 1332–1341. https://doi.org/10.1161/CIRCRESAHA.111.249433

Li, P., Cavallero, S., Gu, Y., Chen, T. H. P., Hughes, J., Hassan, A. B., Brüning, J. C., Pashmforoush, M., & Sucov, H. M. (2011). IGF signaling directs ventricular cardiomyocyte proliferation during embryonic heart development. *Development*, *138*(9), 1795–1805. https://doi.org/10.1242/dev.054338

Liao, J., Zeng, T. B., Pierce, N., Tran, D. A., Singh, P., Mann, J. R., & Szabó, P. E. (2021). Prenatal

correction of IGF2 to rescue the growth phenotypes in mouse models of Beckwith-Wiedemann and Silver-Russell syndromes. *Cell Reports*, *34*(6). https://doi.org/10.1016/j.celrep.2021.108729

Lopez, M. F., Dikkes, P., Zurakowski, D., & Villa-Komaroff, L. (1996). Insulin-like growth factor II affects the appearance and glycogen content of glycogen cells in the murine placenta. *Endocrinology*, *137*(5). https://doi.org/10.1210/endo.137.5.8612553

Love, M. I., Huber, W., & Anders, S. (2014). Moderated estimation of fold change and dispersion for RNA-seq data with DESeq2. *Genome Biology*, *15*(12). https://doi.org/10.1186/s13059-014-0550-8

Marsh, B., & Blelloch, R. (2020). Single nuclei RNA-seq of mouse placental labyrinth development. *ELife*, *9*. https://doi.org/10.7554/eLife.60266

Maslen, C. L. (2018). Recent advances in placenta-heart interactions. *Frontiers in Physiology*, *9*(JUN), 1–9. https://doi.org/10.3389/fphys.2018.00735

Matthiesen, N. B., Henriksen, T. B., Agergaard, P., Gaynor, J. W., Bach, C. C., Hjortdal, V. E., & Østergaard, J. R. (2016). Congenital Heart Defects and Indices of Placental and Fetal Growth in a Nationwide Study of 924 422 Liveborn Infants. *Circulation*, *134*(20), 1546–1556. https://doi.org/10.1161/CIRCULATIONAHA.116.021793

Mi, H., Muruganujan, A., Ebert, D., Huang, X., & Thomas, P. D. (2019). PANTHER version 14: More genomes, a new PANTHER GO-slim and improvements in enrichment analysis tools. *Nucleic Acids Research*, *47*(D1). https://doi.org/10.1093/nar/gky1038

Mootha, V. K., Lindgren, C. M., Eriksson, K. F., Subramanian, A., Sihag, S., Lehar, J., Puigserver, P., Carlsson, E., Ridderstråle, M., Laurila, E., Houstis, N., Daly, M. J., Patterson, N., Mesirov, J. P., Golub, T. R., Tamayo, P., Spiegelman, B., Lander, E. S., Hirschhorn, J. N., … Groop, L. C. (2003). PGC-1α-responsive genes involved in oxidative phosphorylation are coordinately downregulated in human diabetes. *Nature Genetics*, *34*(3). https://doi.org/10.1038/ng1180

Penny, D. J., & Vick, G. W. (2011). Ventricular septal defect. *The Lancet*, *377*(9771), 1103–1112. https://doi.org/10.1016/S0140-6736(10)61339-6

Perez-Garcia, V., Fineberg, E., Wilson, R., Murray, A., Mazzeo, C. I., Tudor, C., Sienerth, A., White, J.

1028 K., Tuck, E., Ryder, E. J., Gleeson, D., Siragher, E., Wardle-Jones, H., Staudt, N., Wali, N., Collins,
1029 J., Geyer, S., Busch-Nentwich, E. M., Galli, A., … Hemberger, M. (2018). Placentation defects are
1030 highly prevalent in embryonic lethal mouse mutants. *Nature*, *555*(7697), 463–468.
1031 https://doi.org/10.1038/nature26002
1032 Poirier, F., Chan, C. T. J., Timmons, P. M., Robertson, E. J., Evans, M. J., & Rigby, P. W. J. (1991). The
1033 murine H19 gene is activated during embryonic stem cell differentiation in vitro and at the time of
1034 implantation in the developing embryo. *Development*, *113*(4).
1035 https://doi.org/10.1242/dev.113.4.1105
1036 Rochais, F., Sturny, R., Chao, C. M., Mesbah, K., Bennett, M., Mohun, T. J., Bellusci, S., & Kelly, R. G.
1037 (2014). FGF10 promotes regional foetal cardiomyocyte proliferation and adult cardiomyocyte cell-
1038 cycle re-entry. *Cardiovascular Research*, *104*(3). https://doi.org/10.1093/cvr/cvu232
1039 Rychik, J., Goff, D., McKay, E., Mott, A., Tian, Z., Licht, D. J., & Gaynor, J. W. (2018). Characterization
1040 of the Placenta in the Newborn with Congenital Heart Disease: Distinctions Based on Type of
1041 Cardiac Malformation. *Pediatric Cardiology*, *39*(6), 1165–1171. https://doi.org/10.1007/s00246-
1042 018-1876-x
1043 Sandovici, I., Georgopoulou, A., Pérez-García, V., Hufnagel, A., López-Tello, J., Lam, B. Y. H.,
1044 Schiefer, S. N., Gaudreau, C., Santos, F., Hoelle, K., Yeo, G. S. H., Burling, K., Reiterer, M.,
1045 Fowden, A. L., Burton, G. J., Branco, C. M., Sferruzzi-Perri, A. N., & Constância, M. (2022). The
1046 imprinted Igf2-Igf2r axis is critical for matching placental microvasculature expansion to fetal
1047 growth. *Developmental Cell*, *57*(1), 63-79.e8. https://doi.org/10.1016/j.devcel.2021.12.005
1048 SanMiguel, J. M., Abramowitz, L. K., & Bartolomei, M. S. (2018). Imprinted gene dysregulation in a
1049 Tet1 null mouse model is stochastic and variable in the germline and offspring. *Development*
1050 *(Cambridge)*, *145*(7). https://doi.org/10.1242/dev.160622
1051 Savolainen, S. M., Foley, J. F., & Elmore, S. A. (2009). Histology atlas of the developing mouse heart
1052 with emphasis on E11.5 to E18.5. *Toxicologic Pathology*, *37*(4), 395–414.
1053 https://doi.org/10.1177/0192623309335060

1054 Schindelin, J., Arganda-Carreras, I., Frise, E., Kaynig, V., Longair, M., Pietzsch, T., Preibisch, S.,
1055 Rueden, C., Saalfeld, S., Schmid, B., Tinevez, J. Y., White, D. J., Hartenstein, V., Eliceiri, K.,
1056 Tomancak, P., & Cardona, A. (2012). Fiji: An open-source platform for biological-image analysis.
1057 In *Nature Methods* (Vol. 9, Issue 7). https://doi.org/10.1038/nmeth.2019
1058 Serra, A., Eirich, K., Winkler, A. K., Mrasek, K., Ghring, G., Barbi, G., Cario, H., Schlegelberger, B.,
1059 Pokora, B., Liehr, T., Leriche, C., Henne-Bruns, D., Barth, T. F., & Schindler, D. (2012). Shared
1060 copy number variation in simultaneous nephroblastoma and neuroblastoma due to Fanconi anemia.
1061 *Molecular Syndromology*, *3*(3), 120–130. https://doi.org/10.1159/000341935
1062 Shen, H., Cavallero, S., Estrada, K. D., Sandovici, I., Kumar, S. R., Makita, T., Lien, C. L., Constancia,
1063 M., & Sucov, H. M. (2015). Extracardiac control of embryonic cardiomyocyte proliferation and
1064 ventricular wall expansion. *Cardiovascular Research*, *105*(3), 271–278.
1065 https://doi.org/10.1093/cvr/cvu269
1066 Shen, H., Gan, P., Wang, K., Darehzereshki, A., Wang, K., Ram Kumar, S., Lien, C. L., Patterson, M.,
1067 Tao, G., & Sucov, H. M. (2020). Mononuclear diploid cardiomyocytes support neonatal mouse heart
1068 regeneration in response to paracrine IGF2 signaling. *ELife*, *9*, 1–24.
1069 https://doi.org/10.7554/eLife.53071
1070 Sibley, C. P., Coan, P. M., Dean, W., Hughes, J., Smith, P., Reik, W., & Burton, G. J. (2004). *Regulates*
1071 *the Diffusional Exchange Characteristics of the Mouse Placenta*. *2*.
1072 Snider, P., & Conway, S. J. (2011). Probing human cardiovascular congenital disease using transgenic
1073 mouse models. In *Progress in Molecular Biology and Translational Science* (1st ed., Vol. 100).
1074 Elsevier Inc. https://doi.org/10.1016/B978-0-12-384878-9.00003-0
1075 Soellner, L., Kraft, F., Sauer, S., Begemann, M., Kurth, I., Elbracht, M., & Eggermann, T. (2019). Search
1076 for cis-acting factors and maternal effect variants in Silver-Russell patients with ICR1
1077 hypomethylation and their mothers. *European Journal of Human Genetics*, *27*(1).
1078 https://doi.org/10.1038/s41431-018-0269-1
1079 Soemedi, R., Wilson, I. J., Bentham, J., Darlay, R., Töpf, A., Zelenika, D., Cosgrove, C., Setchfield, K.,

1080 Thornborough, C., Granados-Riveron, J., Blue, G. M., Breckpot, J., Hellens, S., Zwolinkski, S.,
1081 Glen, E., Mamasoula, C., Rahman, T. J., Hall, D., Rauch, A., … Keavney, B. D. (2012).
1082 Contribution of global rare copy-number variants to the risk of sporadic congenital heart disease.
1083 *American Journal of Human Genetics*, *91*(3). https://doi.org/10.1016/j.ajhg.2012.08.003
1084 Spicer, D. E., Hsu, H. H., Co-Vu, J., Anderson, R. H., & Fricker, F. J. (2014). Ventricular septal defect.
1085 *Orphanet Journal of Rare Diseases*, *9*, 144. https://doi.org/10.1186/s13023-014-0144-2
1086 Subramanian, A., Tamayo, P., Mootha, V. K., Mukherjee, S., Ebert, B. L., Gillette, M. A., Paulovich, A.,
1087 Pomeroy, S. L., Golub, T. R., Lander, E. S., & Mesirov, J. P. (2005). Gene set enrichment analysis:
1088 A knowledge-based approach for interpreting genome-wide expression profiles. *Proceedings of the*
1089 *National Academy of Sciences of the United States of America*, *102*(43).
1090 https://doi.org/10.1073/pnas.0506580102
1091 Sullivan, K. E., & Black, L. D. (2013). The role of cardiac fibroblasts in extracellular matrix-mediated
1092 signaling during normal and pathological cardiac development. *Journal of Biomechanical*
1093 *Engineering*, *135*(7). https://doi.org/10.1115/1.4024349
1094 Thorvaldsen, J. L., Duran, K. L., & Bartolomei, M. S. (1998). Deletion of the H19 differentially
1095 methylated domain results in loss of imprinted expression of H19 and Igf2. *Genes and Development*.
1096 https://doi.org/10.1101/gad.12.23.3693
1097 Thorvaldsen, J. L., Fedoriw, A. M., Nguyen, S., & Bartolomei, M. S. (2006). Developmental Profile of
1098 H19 Differentially Methylated Domain (DMD) Deletion Alleles Reveals Multiple Roles of the
1099 DMD in Regulating Allelic Expression and DNA Methylation at the Imprinted H19/Igf2 Locus.
1100 *Molecular and Cellular Biology*. https://doi.org/10.1128/mcb.26.4.1245-1258.2006
1101 Thorvaldsen, J. L., Mann, M. R. W., Nwoko, O., Duran, K. L., & Bartolomei, M. S. (2002). Analysis of
1102 Sequence Upstream of the Endogenous H19 Gene Reveals Elements Both Essential and Dispensable
1103 for Imprinting. *Molecular and Cellular Biology*. https://doi.org/10.1128/mcb.22.8.2450-2462.2002
1104 Ueno, M., Lee, L. K., Chhabra, A., Kim, Y. J., Sasidharan, R., VanHandel, B., Wang, Y., Kamata, M.,
1105 Kamran, P., Sereti, K. I., Ardehali, R., Jiang, M., & Mikkola, H. K. A. (2013). C-Met-Dependent

Multipotent Labyrinth Trophoblast Progenitors Establish Placental Exchange Interface. *Developmental Cell*, *27*(4), 373–386. https://doi.org/10.1016/j.devcel.2013.10.019

Vega-Hernández, M., Kovacs, A., de Langhe, S., & Ornitz, D. M. (2011). FGF10/FGFR2b signaling is essential for cardiac fibroblast development and growth of the myocardium. *Development*, *138*(15). https://doi.org/10.1242/dev.064410

Von Gise, A., & Pu, W. T. (2012). Endocardial and epicardial epithelial to mesenchymal transitions in heart development and disease. *Circulation Research*, *110*(12), 1628–1645. https://doi.org/10.1161/CIRCRESAHA.111.259960

Vrooman, L. A., Rhon-Calderon, E. A., Chao, O. Y., Nguyen, D. K., Narapareddy, L., Dahiya, A. K., Putt, M. E., Schultz, R. M., & Bartolomei, M. S. (2020). Assisted reproductive technologies induce temporally specific placental defects and the preeclampsia risk marker sFLT1 in mouse. *Development (Cambridge, England)*, *147*(11). https://doi.org/10.1242/dev.186551

Wakeling, E. L., Brioude, F., Lokulo-Sodipe, O., O'Connell, S. M., Salem, J., Bliek, J., Canton, A. P. M., Chrzanowska, K. H., Davies, J. H., Dias, R. P., Dubern, B., Elbracht, M., Giabicani, E., Grimberg, A., Grønskov, K., Hokken-Koelega, A. C. S., Jorge, A. A., Kagami, M., Linglart, A., … Netchine, I. (2017). Diagnosis and management of Silver-Russell syndrome: First international consensus statement. *Nature Reviews Endocrinology*, *13*(2), 105–124. https://doi.org/10.1038/nrendo.2016.138

Wang, Y., Sun, X., & Sun, X. (2021). The Functions of LncRNA H19 in the Heart. In *Heart Lung and Circulation*. https://doi.org/10.1016/j.hlc.2021.10.022

Woods, L., Perez-Garcia, V., & Hemberger, M. (2018). Regulation of Placental Development and Its Impact on Fetal Growth—New Insights From Mouse Models. *Frontiers in Endocrinology*, *9*(September), 1–18. https://doi.org/10.3389/fendo.2018.00570

Yang, H., Wang, H., & Jaenisch, R. (2014). Generating genetically modified mice using CRISPR/Cas-mediated genome engineering. *Nature Protocols*, *9*(8). https://doi.org/10.1038/nprot.2014.134